AD-A092 247 ROCKWELL INTERNATIONAL THOUSAND OAKS CA SCIENCE CENTER F/G 11/6
THE STRAIN ENERGY OF A SPHEROIDAL INCLUSION AND ITS APPLICATION--ETC(U)
JUN 74 M SHIBATA, K ONO N00014-67-C-0439
UNCLASSIFIED TR-10 NL

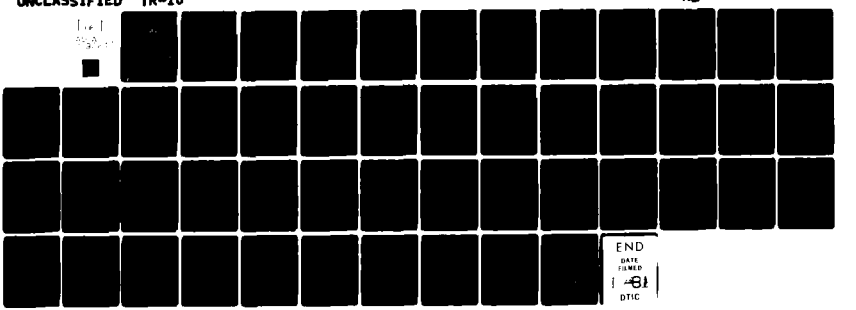

END
DATE FILMED
1-81
DTIC

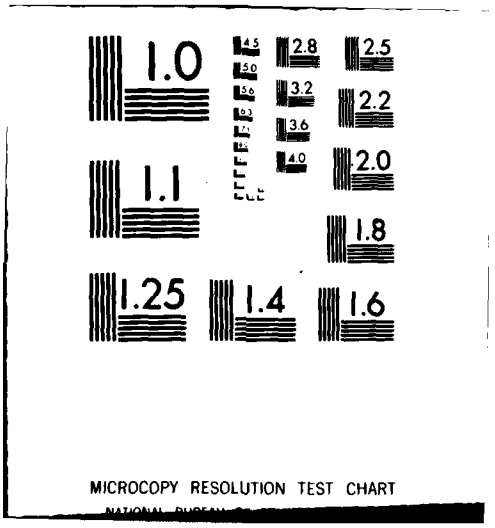
1.0
1.1
1.25
1.4
1.6
1.8
2.0
2.2
2.5
2.8
3.2
3.6
4.0
4.5
5.0
5.6
6.3
7.1
MICROCOPY RESOLUTION TEST CHART

SECURITY CLASSIFICATION OF THIS PAGE (When Date Entered)

REPORT DOCUMENTATION PAGE

READ INSTRUCTIONS BEFORE COMPLETING FORM

1. REPORT NUMBER: ONR Technical Report #10
2. GOVT ACCESSION NO.: AD-A092247
3. RECIPIENT'S CATALOG NUMBER:

4. TITLE (and Subtitle): The Strain Energy of a Spheroidal Inclusion and Its Application to bcc-hcp Martensitic Transformation
5. TYPE OF REPORT & PERIOD COVERED: Technical Report
6. PERFORMING ORG. REPORT NUMBER:

7. AUTHOR(s): M. Shibata and Kanji Ono
8. CONTRACT OR GRANT NUMBER(s): N00014-67-C-4039

9. PERFORMING ORGANIZATION NAME AND ADDRESS: UCLA School of Engineering and Applied Science, Los Angeles, California 90024
10. PROGRAM ELEMENT, PROJECT, TASK AREA & WORK UNIT NUMBERS: NR031-718/2-9/67 (Code 423)

11. CONTROLLING OFFICE NAME AND ADDRESS: Office of Naval Research
12. REPORT DATE: June 1974
13. NUMBER OF PAGES: 48

14. MONITORING AGENCY NAME & ADDRESS (if different from Controlling Office):
15. SECURITY CLASS. (of this report): Unclassified
15a. DECLASSIFICATION/DOWNGRADING SCHEDULE:

16. DISTRIBUTION STATEMENT (of this Report)

This document has been approved for public release and sale, its distribution is unlimited.

17. DISTRIBUTION STATEMENT (of the abstract entered in Block 20, if different from Report)

18. SUPPLEMENTARY NOTES

19. KEY WORDS (Continue on reverse side if necessary and identify by block number)

Titanium Alloy, Martensite, Elastic strain energy, spheroidal inclusion, Bcc-hcp transformation

20. ABSTRACT (Continue on reverse side if necessary and identify by block number)

The strain energy of a spheroidal inclusion was evaluated exactly using the Eshelby theory. Numerical results for an oblate spheroid are presented in a parametric form in terms of the transformation strain tensor. Using atomistic transformation

DD FORM 1 JAN 73 1473 EDITION OF 1 NOV 65 IS OBSOLETE
S/N 0102-014-6601

mechanisms, the transformation strain was determined for bcc-hcp martensitic transformation in Ti and its alloys. The lattice correspondence satisfied the Burgers relationship and the c/a-ratio in the preduct phase was taken as 1.586. The habit plane was predicted on the basis of the strain energy minimization principle. Results of the calculation indicate that the strain energy is minimized when the morphology of hcp Ti martensite is a thin disc-shaped inclusion lying on a plane close to $(9\ 9\ 13)_B$, in excellent agreement with experimental observations.

The present approach is discussed in detail and compared with the crystallographic theory based on the invariant plane strain hypothesis.

UCLA-ENG-7457

(9) Technical Report, No. 10

to

The Office of Naval Research

(15) Contract N00014-67-C-0439 (12) 50

(6) The Strain Energy of a Spheroidal Inclusion and Its Application To bcc-hcp Martensitic Transformation†

(10) M. Shibata and Kanji Ono
MATERIALS DEPARTMENT
School of Engineering and Applied Science
University of California
Los Angeles, California 90024

(11) Jun 74

(14) TR-10

June 1974

Distribution of the Document is unlimited

†Supported by the Metallurgy Program, the Office of Naval Research, through Rockwell International Science Center.

ABSTRACT

The strain energy of a spheroidal inclusion was evaluated exactly using the Eshelby theory. Numerical results for an oblate spheroid are presented in a parametric form in terms of the transformation strain tensor. Using atomisitc transformation mechanisms, the transformation strain was determined for bcc-hcp martensitic transformation in Ti and its alloys. The lattice correspondence satisfied the Burgers relationship and the c/a-ratio in the preduct phase was taken as 1.586. The habit plane was predicted on the basis of the strain energy minimization principle. Results of the calculation indicate that the strain energy is minimized when the morphology of hcp Ti martensite is a thin disc-shaped inclusion lying on a plane close to (9 9 13)$_B$, in excellent agreement with experimental observations.

The present approach is discussed in detail and compared with the crystallographic theory based on the invariant plane strain hypothesis.

1. INTRODUCTION

Because of the technological importance of ferrous martensites, various aspects of martensitic phase transformation have been investigated extensively.[1,2] The phenomenological crystallographic theory of martensite formation was developed in the 1950's and is based on the concept of the invariant habit plane. The theory resolves the total shape deformation, $\bar{F}$, into a pure strain that converts the parent into the product lattice, $\bar{P}$, a lattice invariant shear that produces two undistorted planes, $\bar{S}$, and a rotation that ensures the invariant interface plane, $\bar{R}$. The basic hypothesis of the theory is that the total shape deformation is an invariant plane strain. The whole of the volume change of the transformation is produced as an expansion or contraction normal to the habit plane as well as a small dilatation within the habit plane in the Bowles-Mackenzie (B-M) formulation.[3] The various formulations of the theory were presented by Bowles and Mackenzie,[3] Bullough and Bilby,[4] and Wechsler et al.[5] and in a modified form by Ross and Crocker,[6] et al. These formulations have been successful in accounting for the crystallographic characteristics of many transformations, such as ferrous transformations with the $\{3\ 15\ 10\}_F$ habit plane and the bcc-hcp transformation in Ti and Zr with the $\{334\}_B$ habit plane.[1] However, a variety of martensites are difficult to reconcile with the theory. This group includes ferrous martensites with the habit plane of $\{225\}_F$, $\{259\}_F$, $\{142\}_F$, etc. and Ti martensites with the $\{344\}_B$ habit plane.[1,7] It is also not clear from the theory which factors are responsible for various crystallographic characteristics observed in different alloys.

It is well known that the elastic deformation in the particle of new phase and in the parent lattice controls, to a large extent, a martensitic transformation and the coherent stage of a phase transformation.[8] In the above-mentioned crystallographic theory, it is assumed that a thin plate martensite with the undistorted interfaces satisfies the criterion of a strain energy minimum. This assumption is valid in the cases of plate martensites. Christian[9] considered accommodation strains in the formation of a martensite plate which is an oblate spheroid. The treatment is based on the Eshelby theory of the strain energy in a constrained transformation,[10] but is valid only for a large diameter-to-thickness ratio. His result shows that the strain energy per unit volume tends to zero with an increasing diameter-to-thickness ratio. It is clear that more exact evaluations of the strain energy via a generalized elasticity treatment are necessary in order to develop a new theory that is based on the principle of minimum free energy. Furthermore, the atomistic mechanisms involving dislocations, stacking faults and twins must be integrated into the new theory so that only the probable modes of deformation are to be considered.

In this paper, we establish the correspondence between the crystallographic and Eshelby theories and describe the calculation of the strain energy of spheroidal inclusions using the Eshelby theory. The results are combined with the consideration of atomistic mechanisms in a detailed analysis of martensitic transformation in Ti alloys. It is shown that the results of strain energy minimum determination correlate well with experimental observations on the habit plane. Other features of the present approach is discussed.

2. Theoretical Considerations

2.1 The Eshelby Theory

Eshelby[10] has obtained a general solution for the elastic state of an ellipsoidal inclusion and the matrix, when the inclusion within an isotropic elastic solid undergoes a change of shape and size, which would be homogeneous, but for the contraint imposed by the matrix. Because of the presence of the matrix, internal stresses exist both inside and outside the inclusion. In order to find the elastic field, Eshelby uses a set of five imaginary operations, as shown in Fig. 1. These are

(a) Cut around the inclusion which is to transform and remove it from the matrix,

(b) Allow the transformation to proceed without the constraint; namely, stress-free transformation defined by e_{ij}^{t},

(c) Apply surface tractions to restore the original shape of the inclusion,

(d) Replace the inclusion into the hole in the matrix and rejoin the material across the cut,

(e) Spring back to the self stress state by the release of the surface tractions.

The net effect of these operations is essentially equivalent to the total shape deformation, $\bar{F}$, of the crystallographic theory; that is, Operation b corresponds to the lattice deformation, $\bar{R}\bar{P}$, and Operation c to the lattice invariant shear, $\bar{S}$. Since the crystallographic theory deals with the constrained condition, Operations a and d are omitted. Further the assumption of a very thin plate shape leads to vanishing strain energy so that the relaxation process of Operation e needs not be considered.

On the other hand, only pure shear strain (or its combination) is allowed for $\bar{S}$ in contrast to any homogeneous strain permissible in Operations b and c. This leads to the main distinction between the two approaches. The Eshelby theory provides no shape change after Operations d and a limited shape change or rotation following Operation e, whereas the total shape deformation, $\bar{F}$ is merely reduced to the state of an invariant plane strain in the crystallographic theory.

The total strain energy in matrix and inclusion, E, is obtained by

$$E = \frac{1}{2}\int_{\text{total vol.}} \sigma_{ij}\, e_{ij}\, dV = -\frac{1}{2}\int_{V_I} \sigma_{ij}^{I}\, e_{ij}^{t}\, dv \qquad (1)$$

where σ_{ij}^{I} is the stress in the inclusion, and V_I is the volume of the inclusion, and the summation of repeated indices is implied. In the case of an ellipsoidal inclusion, σ_{ij}^{I} in it is uniform and is given by

$$\sigma_{ij}^{I} = C_{ijk\ell}\left(S_{k\ell mn}\, e_{mn}^{t} - e_{k\ell}^{t}\right) \qquad (2)$$

where the $C_{ijk\ell}$ are the elastic stiffness and the $S_{k\ell mn}$ are the coefficients relating the transformation strain e_{mn}^{t} and the constrained strain $e_{k\ell}^{c}$ by

$$e_{k\ell}^{c} = S_{k\ell mn}\, e_{mn}^{t} \,. \qquad (3)$$

While the evaluation of E is cumbersome, the solution to the elasticity problem of transformation exists in principle. Thus, the remaining tasks are to obtain suitable e_{ij}^{t} for a specific transformation mechanism and to establish a strain energy and free energy minimum condition(s) which depends strongly on geometry.

2.2 The Strain Energy of Spheroidal Inclusions

Eshelby described the general solution for $S_{k\ell mn}$ in terms of elliptic intergrals, from which E can be obtained. To date, however, E's for only few special cases have been evaluated. While the Eshelby theory is valid for general ellipsoids, we shall treat only spheroidal inclusions. This greatly simplifies the calculation without sacrificing the applicability to phase transformation problems. It is also assumed that the elastic constants of the inclusion are identical to those of the matrix and that only one inclusion is present in an infinite media.

This section presents the solutions of E's for several simple cases and a general solution for an oblate spheroidal inclusion. Consider a spheroidal inclusion, the major axes of which coincide with the coordinate axes; namely

$$(x_1/a)^2 + (x_2/b)^2 + (x_3/c)^2 = 1 \tag{4}$$

Two of the constants are identical, e.g., a = c. The aspect ratio k is defined as k = b/a = b/c for this case. Fig. 2 shows such an inclusion with k < 1 (an oblate spheroid). In the expressions below, Poisson's ratio is always taken to be 1/3.

Case 1.

When the only nonzero components of e^t_{ij} are $e^t_{12} = e^t_{21}$, the strain energy E_1 is given by

$$E_1 = \alpha_1 \mu (e^t_{12}) V_I, \quad V_I = \frac{4}{3} \pi abc \tag{5}$$

where α_1 is a constant that depends on the orientation and the aspect ratio of the inclusion and μ is the shear modulus. α_1 can be expressed exactly in terms of elliptic integrals, but approximate expressions for

α_1 are listed in Table I. The range of k where these are valid to within 5% of the exact values is also given on the basis of a comparison with exact calculations.

Case 2.

When all the components of e_{ij}^t except e_{22}^t vanish, the strain energy E_2 is given by

$$E_2 = \alpha_2 \, \mu(e_{22}^t) \quad V_I \, . \tag{6}$$

The approximate expressions for α_2 are tabulated in Table I. E_1 and E_2 have no interaction term so that the sum of the two gives the total strain energy correctly.

Case 3.

When all the elements of e_{ij}^t are nonzero, the strain energy E_3 is given by $\sigma_{ij}^I \, e_{ij}^t \, V_I/2$. When an oblate, spheroidal inclusion with a = c > b exists in the matrix, the strain energy is given by

$$\begin{aligned} E_3 = \mu \, V_I \, \{ & a_1 \left(e_{11}^t + e_{33}^t\right)^2 + a_2 \, e_{11}^t \, e_{33}^t + a_3 \left(e_{11}^t + e_{33}^t\right) e_{22}^t \\ & + a_4 \left(e_{22}^t\right)^2 + a_5 \left[\left(e_{12}^t\right)^2 + \left(e_{23}^t\right)^2 \right] + a_6 \left(e_{13}^t\right)^2 \} \, , \end{aligned} \tag{7}$$

where the numerical values of coefficients a_1 through a_6 are plotted against aspect ratio k(= b/a) in Fig. 3. For oblate, spheroids of different configurations, e.g., a = b > c or a < b = c, E_3 is obtained by interchange of the indices of e_{ij}^t.

TABLE I. STRAIN ENERGY COEFFICIENTS

Geometry	α_1	α_2
$a = b = c$	0.267	0.800
$a < b = c$	$0.980 \times k$ $(k \leq 0.09)$	$1.50 - 1.90 \times k + 3.0 \times k^2$ $(k \leq 0.20)$
$a = c > b$	$0.980 \times k$ $(k \leq 0.09)$	$1.175 \times k$ $(k \leq 0.35)$
$a = b > c$	$0.500 - 0.640 \times k + k^2$ $(k \leq 0.20)$	$1.50 - 1.90 \times k + 3.0 \times k^2$ $(k \leq 0.20)$
$a > b = c$	$0.250 + 0.360 \times k^{-2} + 0.250 \times k^{-2} \times \ell nk$ $(k \geq 3.6)$	$0.563 + 0.175 \times k^{-2} + 0.373 \times k^{-2} \times \ell nk$ $(k \geq 1.2)$
$a = c < b$	$0.250 + 0.360 \times k^{-2} + 0.250 \times k^{-2} \times \ell nk$ $(k \geq 3.6)$	$1.50 + 1.68 \times k^{-2} - 3.00 \times k^{-2}\ \ell nk$ $(k \geq 4.0)$
$a = b < c$	$0.188 + 0.055 \times k^{-2} + 0.125 \times k^{-2} \times \ell nk$ $(k \geq 1.2)$	$0.563 + 0.175 \times k^{-2} + 0.373 \times k^{-2}\ \ell nk$ $(k \geq 1.2)$

2.3 The Present Theory--An Outline

The main objective of this study is to combine the atomistic mechanism of martensitic transformation with the generalized Eshelby treatment. The present theory consists of the following steps:

(i) Determine the transformation strain (e^t_{ij}) based on the lattice correspondence and lattice parameters of the parent and product phase as well as on the probable mode of the e^t_{ij}.

(ii) Evaluate the total strain energy of a spheroidal inclusion and the matrix as a function of the shape and orientation of the inclusion using the Eshelby tensor $S_{ijk\ell}$ obtained from e^t_{ij}.

(iii) Determine the strain energy minimum conditions and the habit orientations. The minimum free energy condition can be deduced by including the interfacial energy term.

Although no restriction is placed on e^t_{ij}, generally e^t_{ij} is decomposed into one or two atomic shear mechanisms and dilatation terms. It is assumed that both the inclusion and matrix are isotropic and homogeneous. In this paper, we describe a specific application of the present theory to martensitic transformation in Ti alloys. Details of the calculation are presented in the following sections.

2.4 The Strain Energy Calculation

When the major axes of a spheroidal inclusion are parallel to the coordinate axes, E can be evaluated by the procedures in Section 2.2, once e^t_{ij} and the inclusion geometry are known. However, these orientations are not necessarily the minimum energy configuration. In order to determine

E for a spheroidal inclusion of arbitrary orientation, the coordinate axes are transformed to coincide the major axes of the inclusion. This requires the simultaneous transformation of e^t_{ij} into the new coordinate system, but enables the subsequent use of the procedures in Section 2.2.

When e^t_{ij} in the original coordinate system is given, the rotation of the coordinate by angle θ about the x_3 axis, as shown in Fig. 4, results in a new strain tensor,

$$(e^t_{ij})_\theta = \begin{pmatrix} \cos\theta & -\sin\theta & 0 \\ \sin\theta & \cos\theta & 0 \\ 0 & 0 & 1 \end{pmatrix} \begin{pmatrix} e_{11} & e_{12} & e_{13} \\ e_{12} & e_{22} & e_{23} \\ e_{13} & e_{23} & e_{33} \end{pmatrix} \begin{pmatrix} \cos\theta & \sin\theta & 0 \\ -\sin\theta & \cos\theta & 0 \\ 0 & 0 & 1 \end{pmatrix} \quad (8)$$

Since the inclusion is spheroidal, another rotation by angle ψ about one of the new coordinate axes, e.g., the x_1' axis, produces the desired re-orientation effect and enables the evaluation of E. However, most of the components of transformation strain in the doubly rotated coordinate system are nonzero and, therefore, the most general formula for E must be used. After the two rotation operations, a new transformation strain tensor is given by

$$(e^t_{ij})_{\theta,\psi} = \begin{pmatrix} 1 & 0 & 0 \\ 0 & \cos\psi & -\sin\psi \\ 0 & \sin\psi & \cos\psi \end{pmatrix} (e^t_{ij})_\theta \begin{pmatrix} 1 & 0 & 0 \\ 0 & \cos\psi & \sin\psi \\ 0 & -\sin\psi & \cos\psi \end{pmatrix} . \quad (9)$$

3. Bcc to hcp Martensitic Transformation

The transformation of high temperature bcc phase of Ti and Zr alloys during quenching is martensitic and results in at least four structures, including hcp, fcc, orthorhombic and fcc orthorhombic.[11] The hcp martensite is most common and occurs in Ti, Zr, Ti-Mo alloys, Zr-Nb alloys

and others. In pure metals and other dilute alloys, the lath martensite forms, whereas the plate martensite occurs with increasing solute content. The habit plane is typically $(334)_B$ or $(8\ 9\ 12)_B$. The orientation relationship of the plate martensite to the matrix has been established to be that due to Burgers,[12] i.e.,

$$(011)_B//(0001)_H,\ [1\bar{1}1]_B//[11\bar{2}0]_H \quad .$$

The experimental orientation relations in Ti and Zr also are close to to the Burgers relationship.

The atomic movements for this transformation can be accomplished by shearing on $(\bar{2}\bar{1}1)_B$ along $[1\bar{1}1]_B$ and a dilation along $[21\bar{1}]_B$ as shown in Fig. 5. The stacking of atoms on $(011)_B$ is identical on every other layer of $(011)_B$ and the illustrated atom movements result in the correct atomic arrangement and stacking sequence of $(0001)_H$. However, the atoms on the middle layer must be moved as well. This is the so-called atomic shuffle, and is ignored in the present theory. This atomistic mechanism was first proposed by Burgers and satisfies the Burgers orientation relationship.[12] When the nearest neighbor distance remains unchanged, an ideal hcp lattice is produced by the atomic movements and the c/a-ratio is 1.633. In the subsequent discussions, we shall always refer to the directions $[1\bar{1}1]_B$, $[\bar{2}\bar{1}1]_B$ and $[011]_B$ as x_1, x_2, and x_3 axes, respectively (cf. Fig. 2). These correspond to the direction of shear, the normal to the plane of shear and the normal to the plane containing all the atomic movements, respectively. In terms of this coordinate system, the transformation strain for the above atomic movements is given by

$$e^t_{ij} = \begin{pmatrix} 0 & .088 & 0 \\ .088 & -.081 & 0 \\ 0 & 0 & 0 \end{pmatrix} . \qquad (10)$$

Since the c/a-ratio of Ti martensite may be approximated by that of pure Ti, 1.586, additional dilatational strain components must be considered. Assuming that the interplanar spacing of $(011)_B$ remains unchanged, the transformation strain for this case becomes

$$e_{ij}^t = \begin{pmatrix} 0.030 & 0.088 & 0 \\ 0.088 & -0.051 & 0 \\ 0 & 0 & 0 \end{pmatrix} . \tag{11}$$

The ratio of lattice parameters of the product and parent lattices, a_H/a_B, is equal to 0.892 in this case, which is slightly smaller than an experimentally observed value of 0.899. The transformation strain of Eq. (11) compares to the one for zirconium obtained by Kelly and Groves,[13] which is given in the present coordinate system as

$$e_{ij}^t = \begin{pmatrix} 0.033 & 0.094 & 0 \\ 0.094 & -0.033 & 0 \\ 0 & 0 & 0.02 \end{pmatrix} . \tag{12}$$

In addition to e_{ij}^t, the uniform rotation ω_{ij}^t accompanies the transformation. In the present case, it is given by

$$\omega_{ij}^t = \begin{pmatrix} 0 & 0.088 & 0 \\ -0.088 & 0 & 0 \\ 0 & 0 & 0 \end{pmatrix} . \tag{13}$$

The sum of e_{ij}^t and ω_{ij}^t is the net distortion β_{ij}^t during the transformation. Note that an atomistic mechanism of phase transformation defines β_{ij}^t, whereas only the e_{ij}^t term of β_{ij}^t is considered in the Eshelby theory.

4. Results

4.1 Simple Cases

When e^t_{ij} is given by Eq. (10) and the coordinate system of Fig. 2 is used, the strain energy is divided into the shear component E_1, and the dilatational component E_2. Using the exact expressions, E_1 and E_2 have been evaluated and are shown as a function of k in Figs. 6 and 7, respectively. The orientation of an oblate spheroid is identified by the normal to the broad face, e.g., $(\bar{2}\bar{1}1)$-disc, whereas that of a prolate spheroid by the long axis, e.g., [110]-needle. Figure 6 shows that the values of E_1 are identical for the $(\bar{2}\bar{1}1)$- and $(\bar{1}1\bar{1})$-discs and for the $[\bar{2}\bar{1}1]$- and $[\bar{1}1\bar{1}]$-needles. E_1 is the lowest for these orientations for disc-like inclusions having small k values, and increases with increasing k up to $k \simeq 2$, after which E decreases slightly. The (011)-disc has the highest E_1, but E_1 for the [011] needles is the lowest among the needles. Figure 7 shows the similar result for E_2. The lowest value is obtained for the $(\bar{2}\bar{1}1)$ disc at vanishing k. Among needle-like inclusions, the $[\bar{1}1\bar{1}]$ and [011] orientations had the lowest values of E_2. E_2 either decreased or increased with raising k for a given orientation. This is in contrast to the strain energy due to dilatation as calculated by Nabarro[14] and shown here by a dashed line. The latter exhibits a maximum for the spherical shape and a minimum for the thin discs.

The total strain energy, $E = E_1 + E_2$, is plotted against k in Fig. 8. The lowest energy configuration corresponds to a thin oblate spheroid with $[\bar{2}\bar{1}1]$ normal to the broad face, or the $[\bar{2}\bar{1}1]$-disc. The second lowest energy configuration is the [011]-needle. The total strain energy for the $[\bar{2}\bar{1}1]$-disc continues to decrease with decreasing k, but that for the [011]-needle approaches the asymptotic value at $k > 5$.

While a suitable selection of parameters is difficult, the effect of the interface energy contribution, E_s can be assessed to a limited degree. Assuming that the volume of an inclusion is 5×10^{-22} cm^3, the interface energy $\gamma = 20$ erg/cm^2, and $\mu = 2 \times 10^{11}$ dyn/cm^2, E_s was evaluated

as a function of k. The total free energy, $E_T = E + E_s$, is shown in Fig. 9. For this small inclusion size, the minimum of E_T exists at k = 0.37 for the $(\bar{2}\bar{1}\bar{1})$-disc.

4.2 The Minimum Strain Energy Configurations

When an oblate spheroid with the broad face normal of $[\bar{2}\bar{1}1]$ (the x_2 axis) is rotated about [011] (the x_3 axis) as shown in Fig. 4; the strain energy of the spheroid varies with the angle or rotation θ and has a two-fold rotational symmetry as shown in Figs. 10 and 11. In both cases, several curves corresponding to different values of k are shown. Figure 10 was obtianed using the transformation strain of Eq. (10), and Fig. 11 using that of Eq. (11), respectively.

Figure 10 represents the strain energy of a spheroidal inclusion transforming to an hcp lattice with the ideal c/a-ratio. The difference between the maximum and minimum values in E tends to vanish with k approaching unity. The minor peak at θ = 150° is much smaller than the peak at θ = 55°. The minimum value of strain energy, E_{min}, and the corresponding value of θ are summarized in Table II. Also shown in the table are the ranges of θ ($\pm\Delta\theta$) within which E differs less than 1% of the strain energy for a spherical inclusion with the identical e^t_{ij}. The strain energy vanishes at θ = 0° or 180° and 115° for k = 0. When k is raised to 0.1, the minimum value of the strain energy increases and two strain energy minima exist at θ = 118 and 176.5°. At k = 0.4 and 0.8, only one broad minimum is found centering at θ = 147°, and E is nearly the same within ±15°. Obviously, no angular dependence exists for the spherical inclusion, k = 1.

TABLE II

Strain Energy Minima

e_{ij}^t	k	$E_{min}/\mu V_I$	θ (degrees)	± Δθ	± Δψ (degrees)
	0	0	115, 180 (or 0)	2	4
Eq. (10)	0.1	3.16×10^{-3}	118, 176.5	3	5
	0.4	8.05×10^{-3}	147	16	8
	0.8	11.9×10^{-3}	147	15	15
	0	0	9, 106	2	4
Eq. (11)	0.1	3.05×10^{-3}	8, 106.5	2	4
	0.4	7.64×10^{-3}	4, 111	6	7
	0.8	9.68×10^{-3}	-20, 120	50	25

When the transformation strain [Eq. (11)] corresponding to the c/a-ratio of 1.586 in the product lattice is used, the angular dependence of the strain energy shown in Fig. 11 was obtained. For the k values less than unity, two strain energy minima always exist, and the minor peak at $\theta = 150°$ is more prominent than in the previous case. As listed in Table II, the minimum strain energy orientations shifted by 9 to 37° between the corresponding values determined using the two e^t_{ij}.

The values of E_{min} on a single curve in Figs. 10 and 11 are identical to each other. The variations of E_{min} with k are shown in Fig. 12. Below $k = 0.1$, the values of E_{min} differ only slightly, but the two curves diverge with increasing k. It is also clear that E_{min} for a given k is lower when e^t_{ij} of Eq. (11) is employed to produce the correct c/a-ratio for titanium than when e^t_{ij} of Eq. (10) is used for the calculation.

Results of the strain energy claculations for a doubly rotated inclusion are summarized in Figs. 13-15. For presentation of voluminous data, the values of strain energy are normalized by the maximum strain energy (E_{max}) for a given e^t_{ij} and k. The magnitude of E is indicated by intergers 1, 2, 3, ... 9, which correspond to $(0.10 \pm 0.01)\ E_{max}$, $(0.2 \pm 0.01)\ E_{max}$, $(0.3 \pm 0.01)\ E_{max}$, ... $(0.0 \pm 0.01)\ E_{max}$, respectively. The locations corresponding to $\left(1.0 \overset{+\ 0.00}{-\ 0.01}\right) E_{max}$ are indicated by asterik (*) marks, while that of E_{min} is given by a plus (+) mark. Figs. 13 and 14 show the positions of various levels of E as a function of θ and ψ, which are taken at 5° intervals. In terms of the standard

stereographic projection, θ corresponds to the longitude and ψ to the latitude; i.e., $\psi = 0$ indicates the equator and $\psi = \pm 90°$, the North and South poles of a Wulff net. Fig. 13 presents the mapping of E for the case when the e^t_{ij} of Eq. (10) is used. The values of k, $E_{max}/\mu V_I$ and $E_{min}/\mu V_I$ are also given, and k is zero for Fig. 13a and is 0.1 for Fig. 13b, respectively. Similar mappings for the e^t_{ij} of Eq. (11) with k = 0, 0.1, 0.4 and 0.8, respectively, are shown in Figs. 14a through 14d. More detailed mappings are shown in Figs. 15a and 15b, which present the normalized values of E for the range of $-10° \leq \theta \leq 20°$ and $|\psi| \pm 10°$ at 1° intervals. The magnitude of E is given by an integer between 0 and 1000, where the latter corresponds to the E value at $\theta = -10°$ and $\psi = \pm 10°$.

From Figs. 13 and 14, it can be seen that the strain energy minima appear only at the locations predicted in Figs. 10 and 11 with $\psi = 0$. However, the low energy orientation spreads over a range of θ and ψ from the minimum energy orientation. This is best illustrated in Figs. 15a and b. E_{min} is located at $\theta = 9°$ and $\psi = 0$, but within the region of $\Delta\theta = \pm 2°$ and $\Delta\psi = \pm 4°$, the value of E increases over E_{min} less than 1% of E of a sphere with the identical e^t_{ij} and V_I. The corresponding ranges of $\Delta\theta$ and $\Delta\psi$ for other values of k and e^t_{ij} are listed in Table II. For the two choices of e^t_{ij} employed, the low energy orientation for thin discs ($k \leq 0.1$) is located over a wider range of ψ than that of θ.

5. Discussion

5.1 Effects of Rotational Components

When the transformation strain e^t_{ij} is given, Eshelby[10] showed that the uniform rotation $\omega^c_{ij} = \frac{1}{2}(u^c_{i,j} - u^c_{j,i})$ in the inclusion is written as

$$\omega^c_{ij} = \Pi_{ijk\ell}\, e^t_{k\ell}. \tag{14}$$

The only non-zero components of $\Pi_{ijk\ell}$ are Π_{1212}, Π_{2323}, Π_{1313} in a coordinate system whose axes coincide the principal axes of the ellipsoidal inclusion. These are given in terms of elliptic intergrals by, e.g.,

$$\Pi_{1212} = -\Pi_{2112} = (I_b - I_a)/8\pi \quad . \tag{15}$$

Since the rotational components of the transformation distortion must be substracted in order to apply the Eshelby theory, the uniform rotation in the inclusion from the original lattice, ω^I_{ij}, is given by

$$\omega^I_{ij} = \omega^c_{ij} - \omega^t_{ij} \quad . \tag{16}$$

This rotational term must be considered in comparing the results of the previous section to the crystallographic orientations determined by experiment.

In both the e^t_{ij} employed in the above calculations of E, the only non-zero contribution to ω^c_{ij} arises from $e^t_{12} = e^t_{21} = 0.088$, and is

$$\omega^c_{12} = -\omega^c_{21} = 2\, e^t_{12}\, \Pi_{1212} - e^t_{12} \quad . \tag{17}$$

The angle of rotation ϕ_3 about x_3 axis becomes

$$\phi_3 = \tan^{-1}(-\omega_{12}^I) \quad . \tag{18}$$

The numerical results are given in Table III, which shows that the rotational correction amounts to only 1.05° for k = 0.1, and vanishes for k = 0.

TABLE III

Rotational Corrections (for $e_{12}^t = 0.088$)

k	Π_{1212}	ω_{12}^I	ϕ_3 (degrees)
0	0.5000	0.0	0.0
0.1	0.3956	-1.837×10^{-2}	1.05
0.4	0.1912	-5.436×10^{-2}	3.11
0.8	0.0458	-7.994×10^{-2}	4.57

5.2 Habit Planes and Shape Deformation

The minimum strain energy configuration of a spheroidal inclusion corresponds to the most likely geometry of the new phase, when the interface energy contribution to the nucleation process can be ignored. If the interface energy contributes significantly, its effect must be evaluated as was done in Section 4.1. However, the orientation dependence of the interface energy is generally unknown. If the interface energy is assumed to be independent of orientation, the most favored

orientation of the new phase is essentially governed by the strain energy except for the fact that an optimum value of the aspect ratio exists where the sum of the strain energy and interface energy contributions is minimized.

Considering the transformation strain of Eq. (11) that corresponds to the c/a-ratio of 1.586 for the product phase, the strain energy minimum exists, when the broad face of the spheroidal inclusion (k = 0) is parallel to $(9\ 9\ 13)_B$. When the aspect ratio is increased to 0.1, the minimum strain energy orietation is shifted by 4° to $(9\ 9\ 14)_B$ including the effect of ϕ_3. These orientations are shown in Fig. 16a together with the ranges of orientations where E increases over E_{min} less than 1% of E of a sphere with identical e_{ij}^T and V_I. These ranges are shown by a hatched area (k = 0) and by a shaded area (k = 0), respectively. The present result of $(9\ 9\ 13)_B$ habit plane is almost identical to experimentally determined habit planes obtained by Newkirk and Geisler[15] and by Liu.[16] The observed habit plane orientations are indicated in Fig. 16b by a filled triangle [the $(8\ 8\ 11)_B$ orientation] and by a hatched area, respectively. The range of observed habit plane orientations shown by a shaded area is due to Gaunt and Christian,[17] whereas a double circle represents the result of Williams et al. [the $(8\ 9\ 12)_B$ orientation][18] and a filled square that of van Ginneken,[19] [the $(569)_B$ orientation]. All the observed habit plane orientations are within a few degrees of the predicted low energy regions, indicating an excellent agreement between theory and experiment. It is also significant that the predicted orientations of low strain energy are not confined to a narrow zone. This is again in accord with experiment, since it has been recognized that the observed scatter of habit planes is beyond the limit of experimental error.

The predicted habit plane of the Bowles-Mackenzie analysis for pure titanium is $(8\ 9\ 12)_B$[20] and agrees with the observed one reported by Williams et al.[18] However, the agreement hinges upon a suitable choice of the adjustable dilatation parameter, which amounts to 0.7%. The lattice invariant shear plane in the above analysis is $\{10\bar{1}1\}_H$. Twins on $\{10\bar{1}1\}_H$ in Ti martensite have been indeed observed by transmission electron microscopy, but their thickness is of such magnitude that it is difficult to interpret them as the lattice invariant shear.[11] The Bowles-Mackenzie prediction of the habit plane is rather close to the predicted low energy orientations of the present analysis. This is perhaps not surprising since it is expected that the invariant plane strain condition postulated by the Bowles-Mackenzie analysis should approximate the strain energy minimum condition.

The total shape distortion in the new phase, β_{ij}^T, is given by the sum of e_{ij}^C and ω_{ij}^I in the present analysis. For the above case where e_{ij} of Eq. (11) is used, β_{ij}^T becomes

$$\beta_{ij}^T = \begin{pmatrix} 0 & 0.088 & 0 \\ 0.088 & -0.036 & 0 \\ 0 & 0 & 0 \end{pmatrix} \tag{20a}$$

for the case of k = 0 and

$$\beta_{ij}^T = \begin{pmatrix} 0.005 & 0.056 & 0 \\ 0.092 & -0.037 & 0 \\ 0 & 0 & 0 \end{pmatrix} \tag{20b}$$

for the case of k = 0.1.

The sum of β_{ij}^T and an identity matrix corresponds to the total shape deformation $\bar{P}$ in the crystallographic theory. As a comparison, β_{ij}^T obtained from the analysis on pure Ti by Bowles and Mackenzie[20] is given in the same coordinate system by

$$\beta_{ij}^T = \begin{pmatrix} -0.1075 & -0.0618 & 0.0709 \\ 0.0550 & 0.0268 & -0.0388 \\ -0.0658 & 0.0405 & 0.0394 \end{pmatrix} \quad (21)$$

It is clear that β_{ij}^T in the Bowles-Mackenzie analysis is not optimized for the strain energy minimum, as the strain components of β_{ij}^T are almost universally greater than those of e_{ij}^c in the present analysis. A comparison of the two β_{ij}'s indicates that, although the net dilatation ($\beta_{11}^T + \beta_{22}^T + \beta_{33}^T$) differs only slightly, a large contraction along the $[1\bar{1}1]_B$ and a substantial expansion along the $[011]_B$ are present in the β_{ij}^T for the Bowles-Mackenzie analysis [Eq. (21)]. The corresponding dilatation parameters in the present analysis are zero. The origin of such a difference can be traced to the processes of lattice transformation in the crystallographic theory, where the invariant plane strain condition is accomplished by adjusting the dilatational strain components. This approach is in a sharp contrast to the present one where the transformation strain is chosen by minimizing atomic movements involved. It is also evident that the dislocation concept of shear transformation is completely absent in the lattice transformation stage of the crystallographic theory. It is invoked only during the lattice invariant shearing. This is why it is so difficult to reconcile the crystallographic theory with the atomistic

or dislocation concept of martensitic transformation. The former achieves the lattice transformation via pure strain (e.g., the Bain distortion), whereas the latter contends the major changes to be due to the motion of transformation dislocations. In the present theory, e^t_{ij} arises from the atomistic concept, which is therefore an integgral part of the theory.

5.3 Needle- and Lath-Type Precipitates of α-Ti

When a concentrated solution of Ti with Mo, V and other so-called β-stabilizers is solution-treated and aged in a α + β phase region, needle- and lath-type precipitates of α-Ti are found in the α-Ti matrix. The long axis of these precipitates is aligned along $\langle 110 \rangle_B$, and the Burgers relationship is satisfied in most of the instances investigated.[11] When the aging was performed at relatively low temperatures (430-480°C for a Ti-18Mo alloy and 480-540°C for Beta-III Ti alloy), Rosales[21] also noted that the alloy partitioning considerably lags behind the β to α transformation and suggested a shear transformation mechanism. Since the lattice correspondence is identical, the present analysis also applies to the α-precipitation. The results presented in Section 4.1 indicate that, while a disc-shaped inclusion has the lowest strain energy, a needle-shaped inclusion along $\langle 110 \rangle_B$ are the preferred geometry. It is not known what causes the needle- and lath-type precipitates to be most stable, but it is naturally expected that the diffusion of solute atoms, the nature of nucleation sites such as grain boundaries, the structure of α-β phase boundaries and precipitate growth mechanism have as much influence as the strain energy. The k-dependence of E as shown in Figs. 6-9, however,

presents one possible explanation. If the nuclei of α-precipitates have semispherical geometry as proposed by Rosales,[21] the growth of $\langle 110 \rangle_B$-needles is preferred over that of $\langle 112 \rangle_B$-discs according to the present results (cf. Fig. 8). This is due to a higher value of -dE/dk for the needle geometry in comparison to that for the disc geometry when k is close to unity; that is, the rate of reduction of E is greater for the growth of $\langle 110 \rangle_B$-needles.

5.4 General Discussion

The theory described in this paper represents a significant departure from the crystallographic theory or from the interface dislocation models.[22,23] It combines the atomistic transformation mechanism based on dislocation movement and the crystallographic features of transformation through the suitable selection of the transformation strain tensor. The theory can be extended to othermartensitic transformations, some of which are being investigated by the present authors.

The present theory can be refined by considering the elastic constants of an inclusion, which differ from those of the matrix. This refinement can be done within the framework of the Eshelby theory.[10] The next extension of the theory will involve the consideration of elastic anisotropy. The general theory for anisotropic inclusion problems has been developed by Kinoshita and Mura.[24] Although a few specific solutions for a spheroidal inclusion have been reduced to line integrals,[25] these are not immediately applicable to martensitic transformation problems. This is due to the symmetry requirement for the elastic constants. Only the spheroidal inclusions whose major axes coincide with the cube axes can be treated by the solutions available.

An entirely different approach to the transformation problem has been developed by Khachaturyan.[8] The theory utilizes the computation of elastic strain energy in the reciprocal space. A general solution is obtained for an inclusion problem in the anisotropic elasticity and a specific solution is given for a tetragonal dilatation in the cubic symmetry. A similar approach has been successful in the analysis of the omega transformation in Ti and Zr alloys.[26,27] However, the application of this theory to martensitic transformation problems requires a substantial effort in the future.

6. Conclusions

1. The total strain energy in matrix and a spheroidal inclusion is determined by using the Eshelby theory. Approximate formulae and a parametric expression for E are obtained by evaluating elliptic integrals. Numerical results for an oblate spheroid are included for the most general form of the transformation strain, e_{ij}^{t}.

2. The atomistic transformation mechanism is combined with the Eshelby theory to provide a new approach to the analysis of martensitic transformation. The correspondence and distinctions between this new theory and the phenomenological crystallographic theory are clarified.

3. Specific e_{ij}^{t} for the bcc-to-hcp transformation in Ti and its alloys is obtained. The habit plane is predicted on the basis of the strain energy (and interface energy) minimization principle. The results are in excellent agreement with experiment.

7. Acknowledgement

The authors are grateful for the support of this research by the Metallurgy Program, the Office of Naval Research, administered through Rockwell International Corporation. They wish to thank Dr. J.C. Williams of Rockwell International Science Center for valuable discussions, and for his contributions as the program manager.

REFERENCES

1. a) B.A. Bilby and J.W. Christian, The Mechanism of Phase Transformation in Metals, The Institute of Metals, London, 1956, p. 121.

   b) J.W. Christian, The Theory of Transformations in Metals and Alloys, Pergamon Press, Oxford, 1965, pp. 802-931.

   c) C.M. Wayman, Introduction to the Crystallography of Martensitic Transformations, Macmillan Company, New York, 1964.

   d) R.P. Reed and J.F. Breedis, Behavior of Metals at Cryogenic Temperatures, ASTM-STP387, Am. Soc. Testing Mats., Philadelphia, 1966, p. 60.

2. "Invited Papers from Symposium on the Formation of Martensite in Iron Alloys," Met. Trans. 2, 2327-2494 (1971).

3. J.S. Bowles and J.K. Mackenzie, Acta Met. 2, 129 (1954).

4. R. Bullough and B.A. Bilby, Proc. Phys. Soc. B69, 1276 (1956).

5. M.S. Wechsler, D.S. Lieberman and T.A. Read, Trans. AIME 197, 1503 (1953).

6. N.D.H. Ross and A.G. Crocker, Acta Met. 18, 405 (1970).

7. D.P. Dunne and C.M. Wayman, Met. Trans. 2, 2327 (1971).

8. A.G. Khachaturyan, Soviet Phys.-Solid State 8, 2163 (1967).

9. J.W. Christian, Acta Met. 6, 377 (1958).

10. J.D. Eshelby, Proc. Roy. Soc. A241, 376 (1957).

11. J.C. Williams, Titanium, Science and Technology, R.I. Jaffee and H.M. Burte (Eds.), Vol. 3, Plenum Press, New York, 1973, p. 1433.

12. W.G. Burgers, Physica 1, 561 (1934).

13. A. Kelly and G.W. Groves, Crystallography and Crystal Defects, Addison-Wesley, Reading, 1970, p. 313.

14. F.R.N. Nabarro, Proc. Phys. Soc. 52, 90 (1940); Proc. Roy. Soc. A175, 519 (1940).

15. J.B. Newkirk and A.H. Geisler, Acta Met. 1, 370 (1953).

16. Y.C. Liu, Trans. AIME 206, 1036 (1956).

17. P. Gaunt and J.W. Christian, Acta Met. 7, 534 (1959).

18. A.J. Williams, R.W. Cahn and C.S. Barrett, Acta Met. 2, 117 (1954)

19. A.J.J. van Ginneken, Acta Cryst. 5, 548 (1952).

20. J.K. Mackenzie and J.S. Bowles, Acta Met. 5, 137 (1957)

21. L.A. Rosales, Ph.D. Thesis, University of California, Los Angeles, (1973).

22. F.C. Frank, Acta Met. 1, 15 (1953).

23. H. Suzuki, Sci. Rept. Tohoku University, Sendai 6, 30 (1954)

24. N. Kinoshita and T. Mura, phys. stat. sol. (a) 5, 759 (1971).

25. S.C. Lin and T. Mura, phys. stat. sol. (a) 15, 281 (1973).

26. H. Cook and D. deFontaine, Acta Met. 17, 915 (1969); 18, 189 (1970).

27. D. deFontaine, N.E. Paton and J.C. Williams, Acta Met. 19, 1153 (1971).

FIGURE CAPTIONS

Fig. 1 Schematic representation of the Eshelby theory[10] and the corresponding processes in the crystallographic theory.[1a]

Fig. 2 Coordinate axes employed and an oblate spheroid with the broad face $//(\bar{2}\bar{1}1)_B$.

Fig. 3 Strain energy coefficients for an oblate spheroidal inclusion.

Fig. 4 The rotation of the coordinate axes about the x_3 axis.

Fig. 5 Atomic arrangements on $\{110\}_B$, $\{110\}_B$ after shearing and $(0001)_H$. Burgers relationship is maintained in the atomic movement.

Fig. 6 Strain energy E_1 due to a shear component e^t_{12} against k.

Fig. 7 Strain energy E_2 due to a dilatation component e^t_{22} against k.

Fig. 8 Total strain energy E against k. e^t_{ij} of Eq. (10) was used and E is expressed in terms of e^t_{12}.

Fig. 9 The sum of E and the interfacial energy, E_T, against k.

Fig. 10 The variation of E due to rotation about the x_3 axis, using e^t_{ij} of Eq. (10). k values are given in the figure, and $\theta = 0$ corresponds to $[\bar{2}\bar{1}1]$-disc and $\theta = 90°$ to $[1\bar{1}1]$-disc.

Fig. 11 The variation of E due to rotation about the x_3 axis, using e^t_{ij} of Eq. (11).

Fig. 12 The k-dependence of E_{min}. e^t_{ij} used is indicated.

Fig. 13 The strain energy mapping with respect to θ and ψ. e^t_{ij} is given by Eq. (10). E_{max} locations are given by (*) and E_{min} by (+). (a) k = 0 (b) k = 0.1.

Fig. 14 The strain energy mapping using e^t_{ij} of Eq. (11). (a) k = 0, (b) k = 0.1 (c) k = 0.4 (d) k = 0.8.

Fig. 15 Details of Figs. 14a and b, in the vicinity of $\theta = \psi = 0$.

Fig. 16 (a) Habit planes predicted by the present theory
(b) Experimentally determined habit planes.

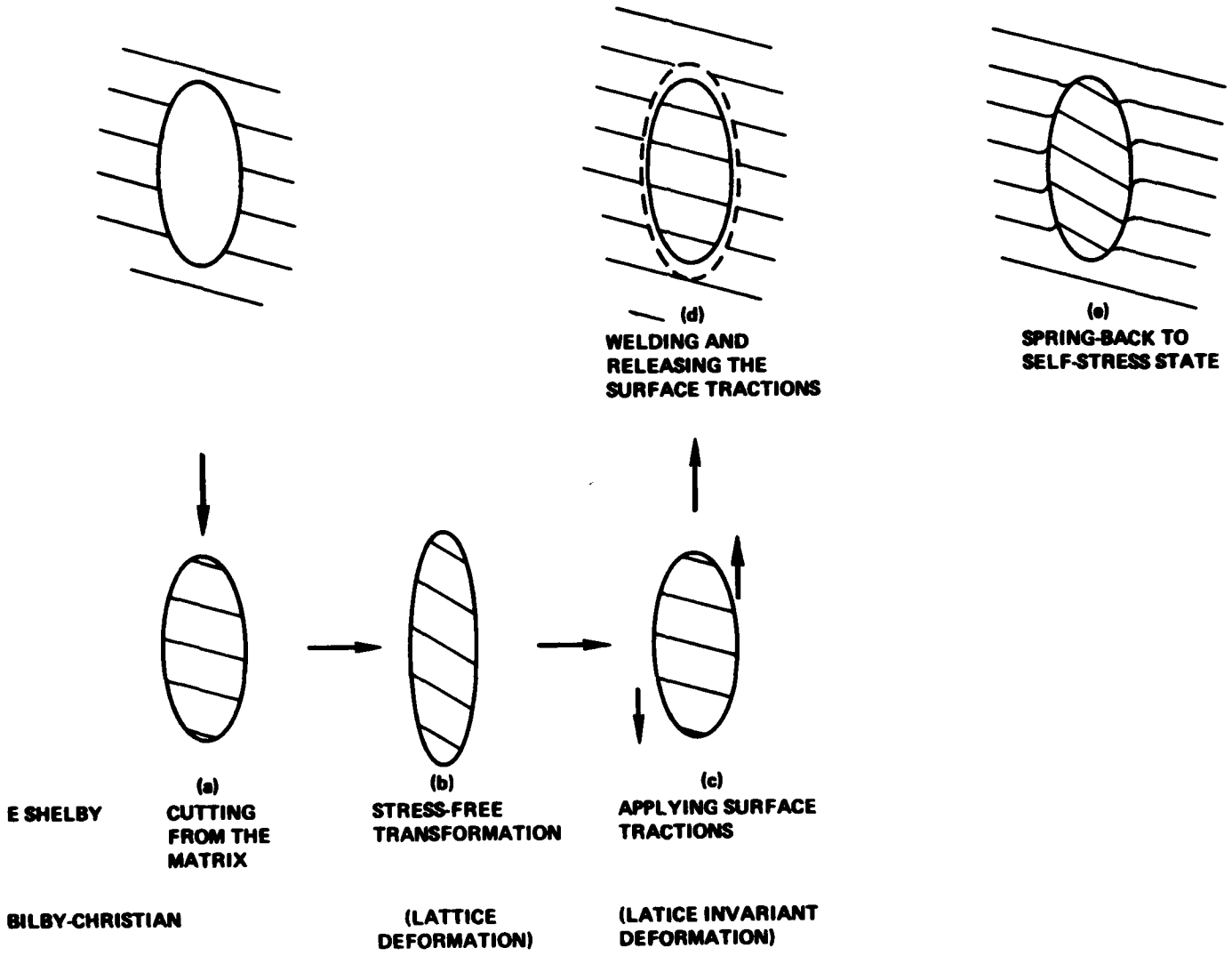

Fig. 1 Schematic representation of the Eshelby theory[10] and the corresponding processes in the crystallographic theory.[1a]

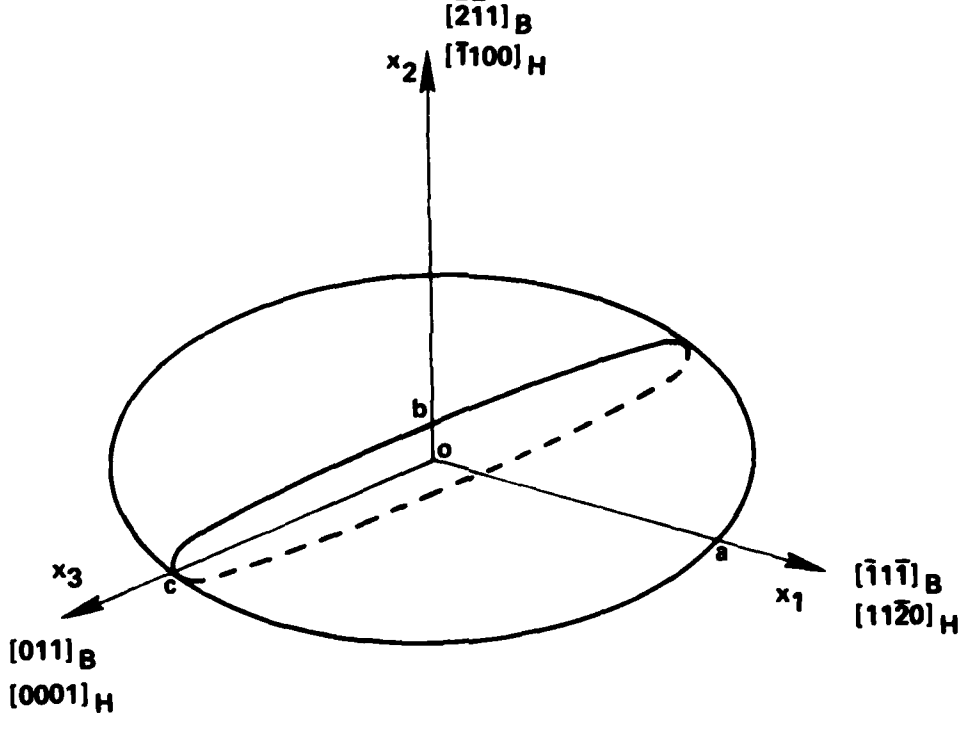

Fig. 2 Coordinate axes employed and an oblate spheroid with the broad face $//(\bar{2}\bar{1}1)_B$.

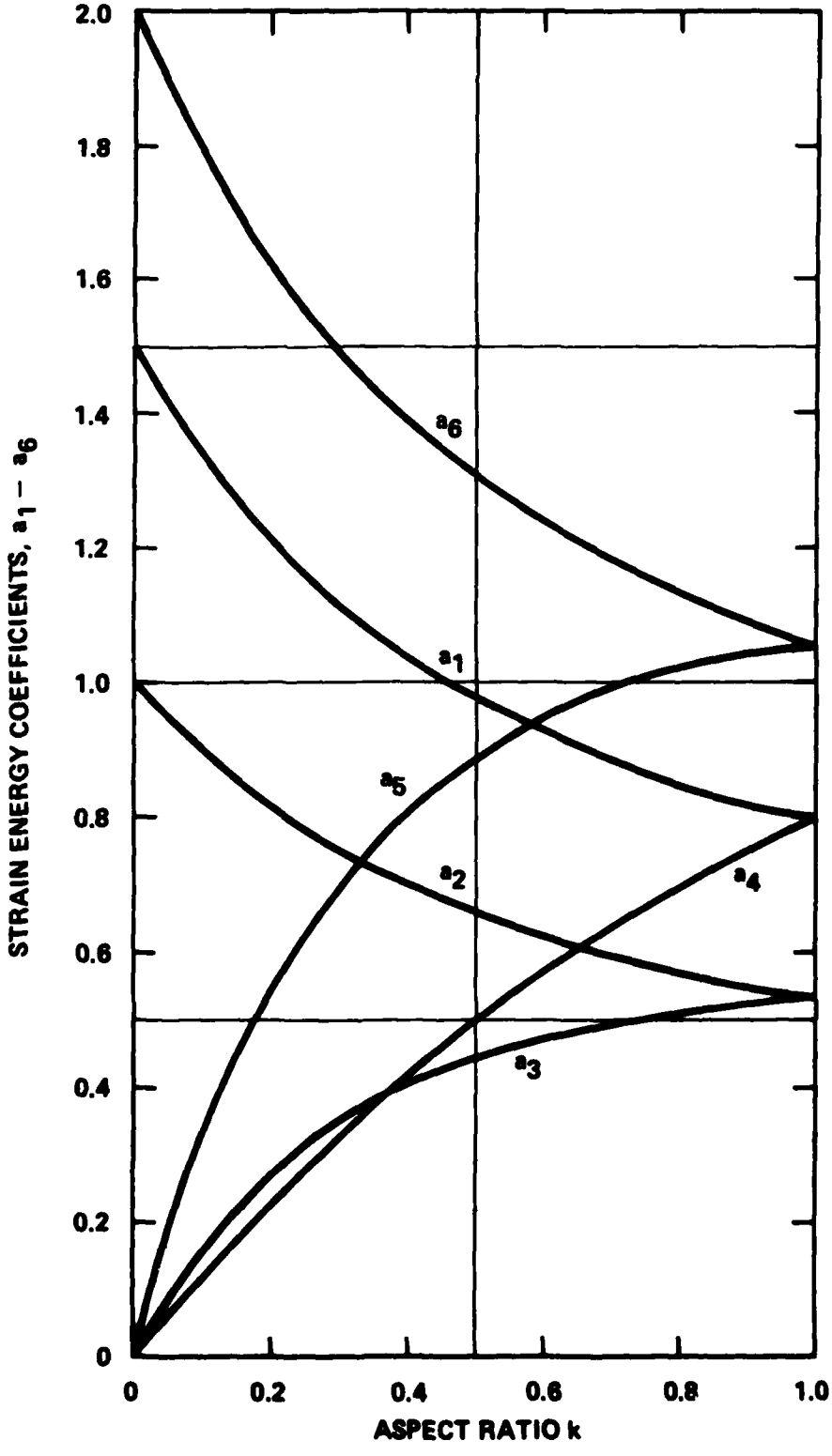

Fig. 3 Strain energy coefficients for an oblate spheroidal inclusion.

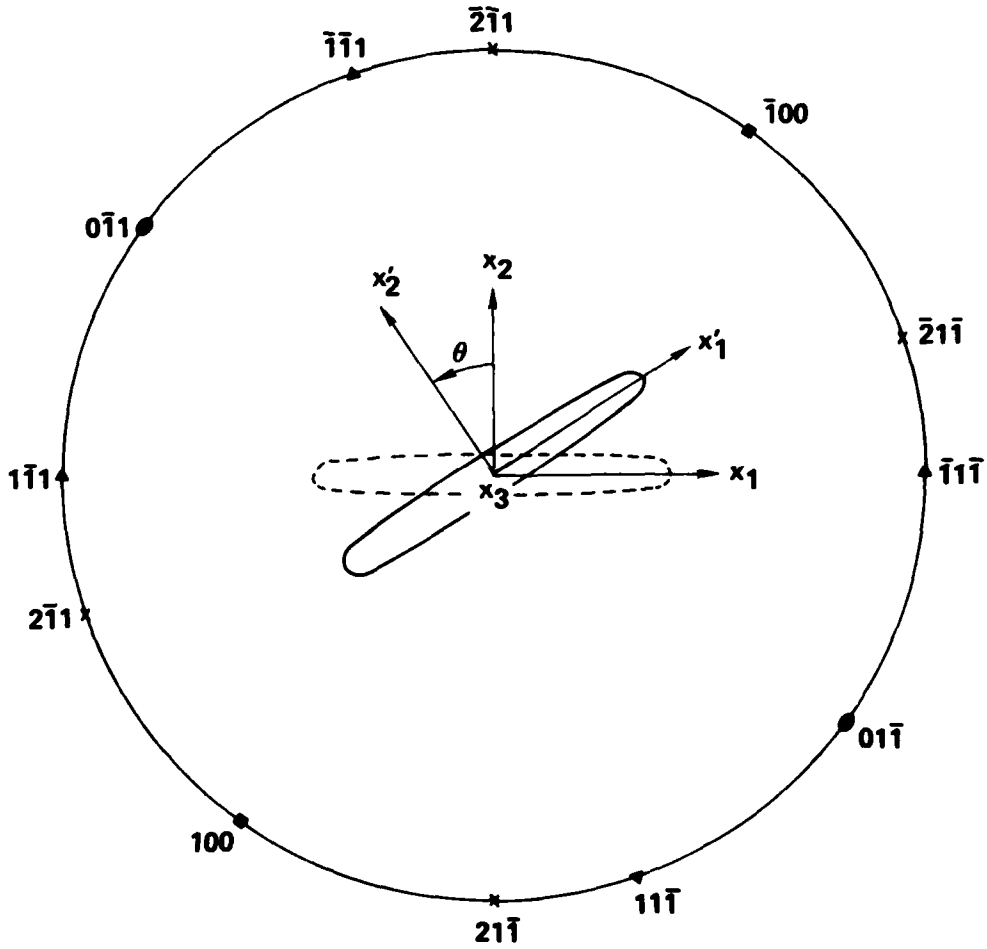

Fig. 4 The rotation of the coordinate axes about the x_3 axis.

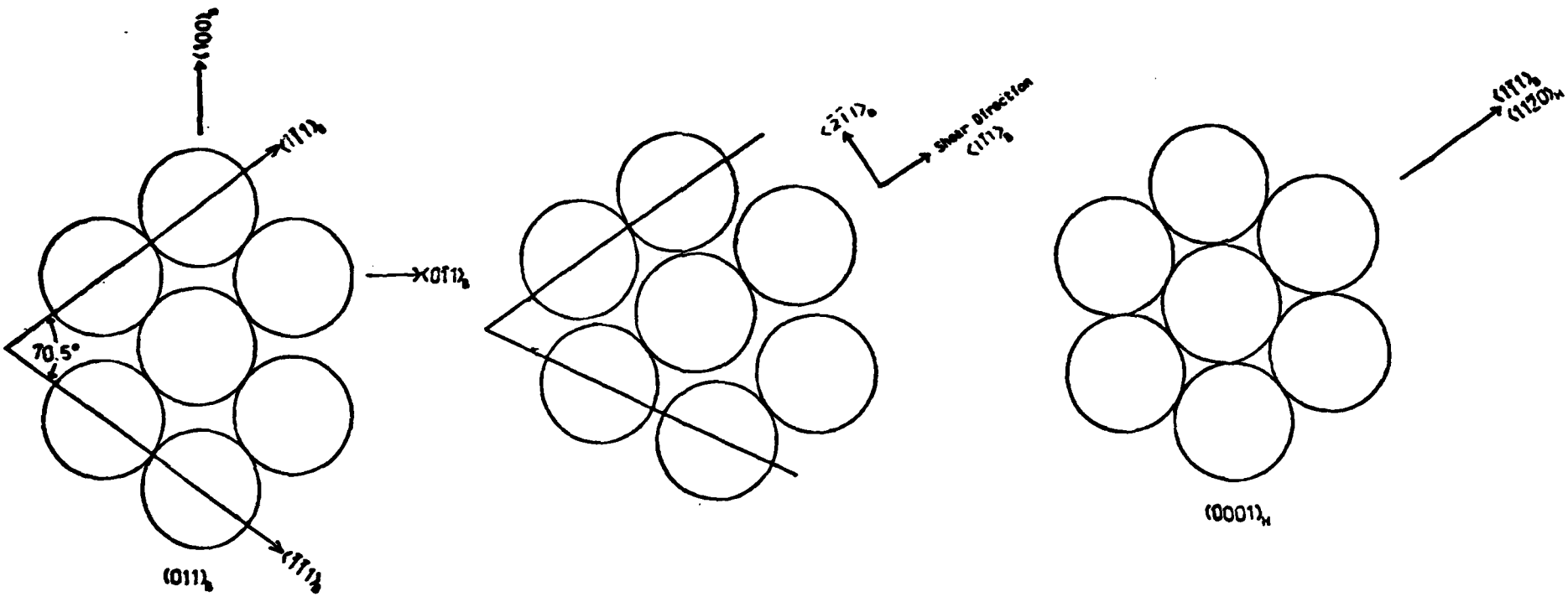

Fig. 5 Atomic arrangements on $\{110\}_B$, $\{\bar{1}10\}_B$ after shearing and $(0001)_H$. Burgers relationship is maintained in the atomic movement.

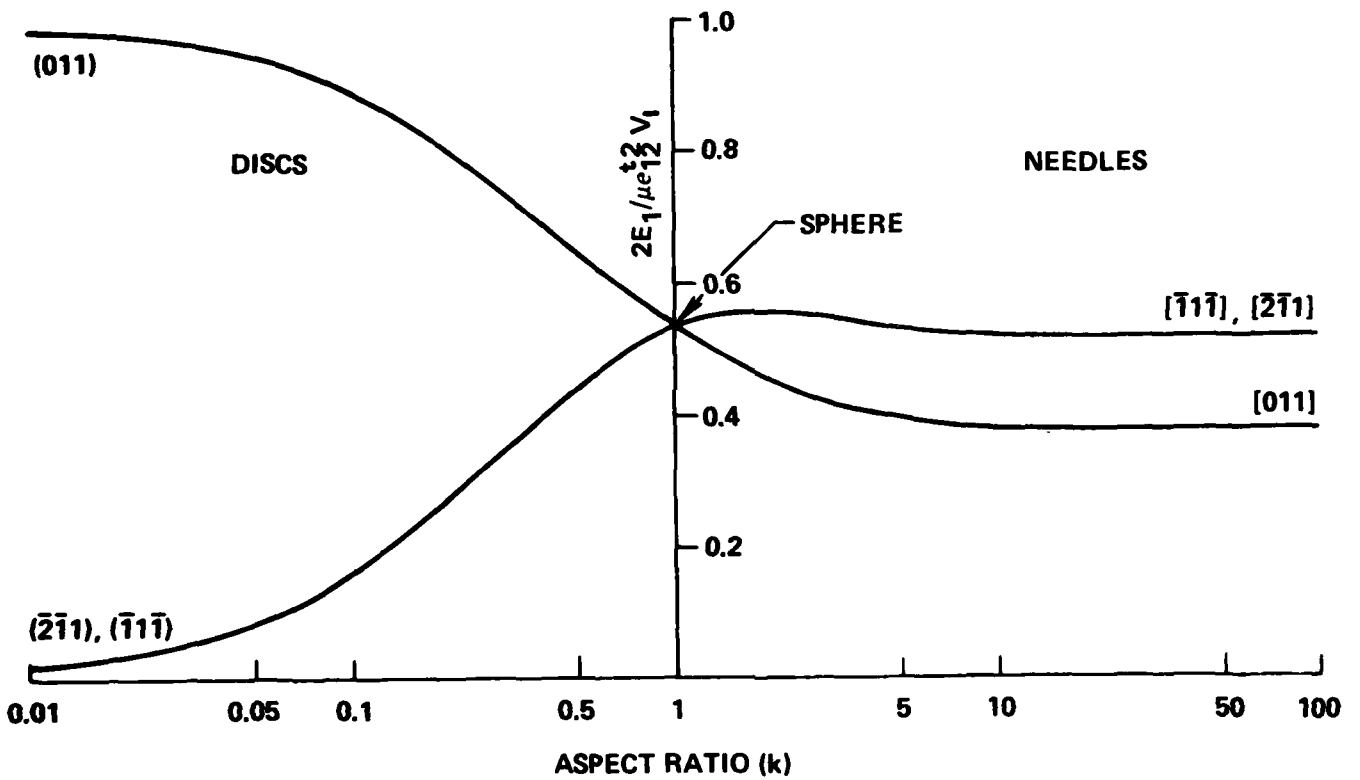

Fig. 6 Strain energy E_1 due to a shear component e_{12}^t against k.

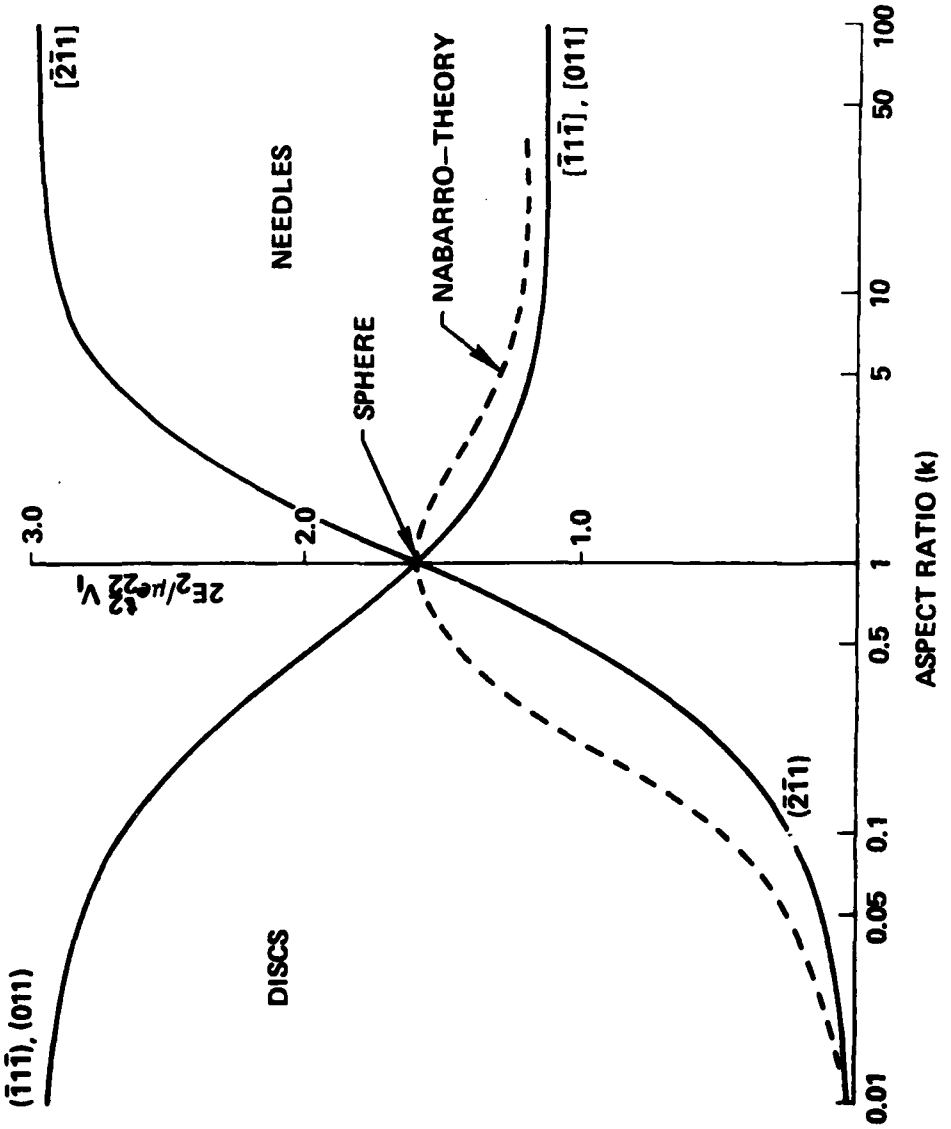

Fig. 7 Strain energy E_2 due to a dilatation component e_{22}^t against k.

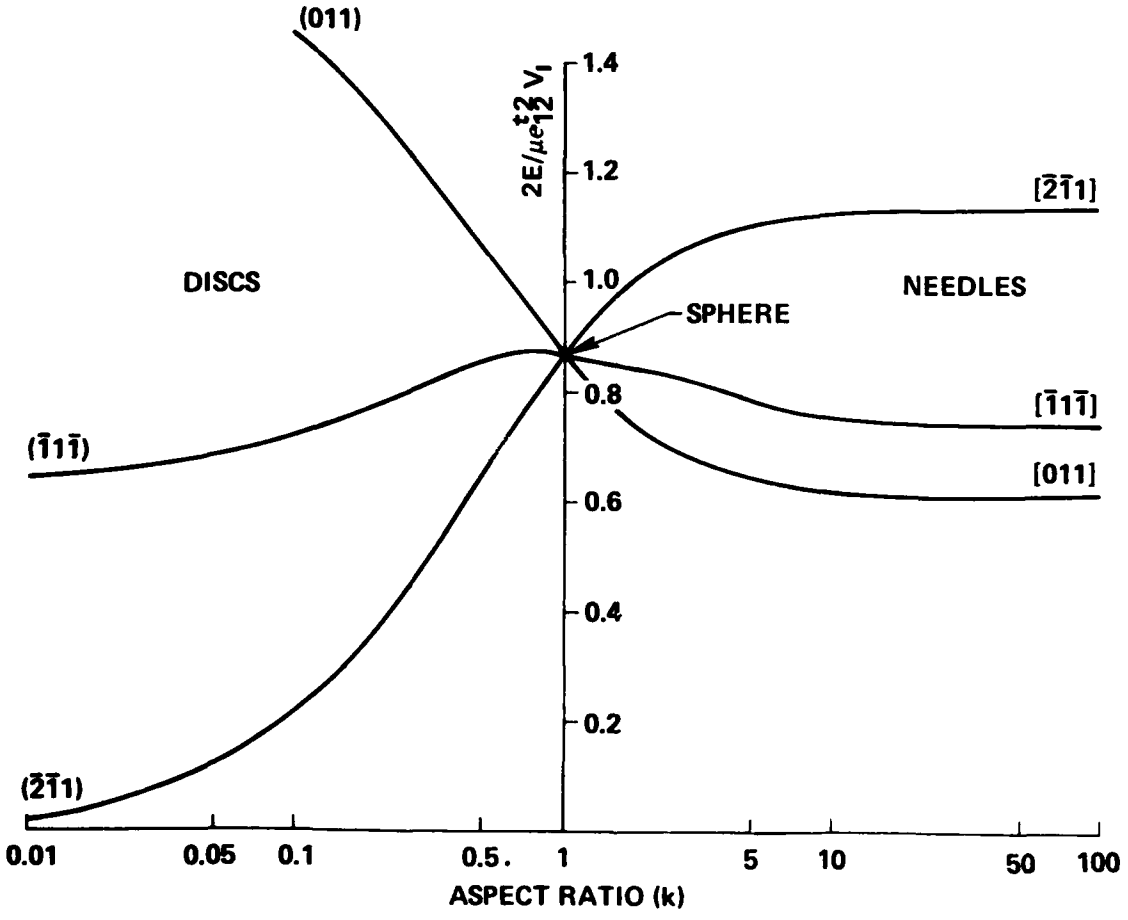

Fig. 8 Total strain energy E against k, e_{ij}^{t} of Eq. (10) was used and E is expressed in terms of e_{12}^{t}.

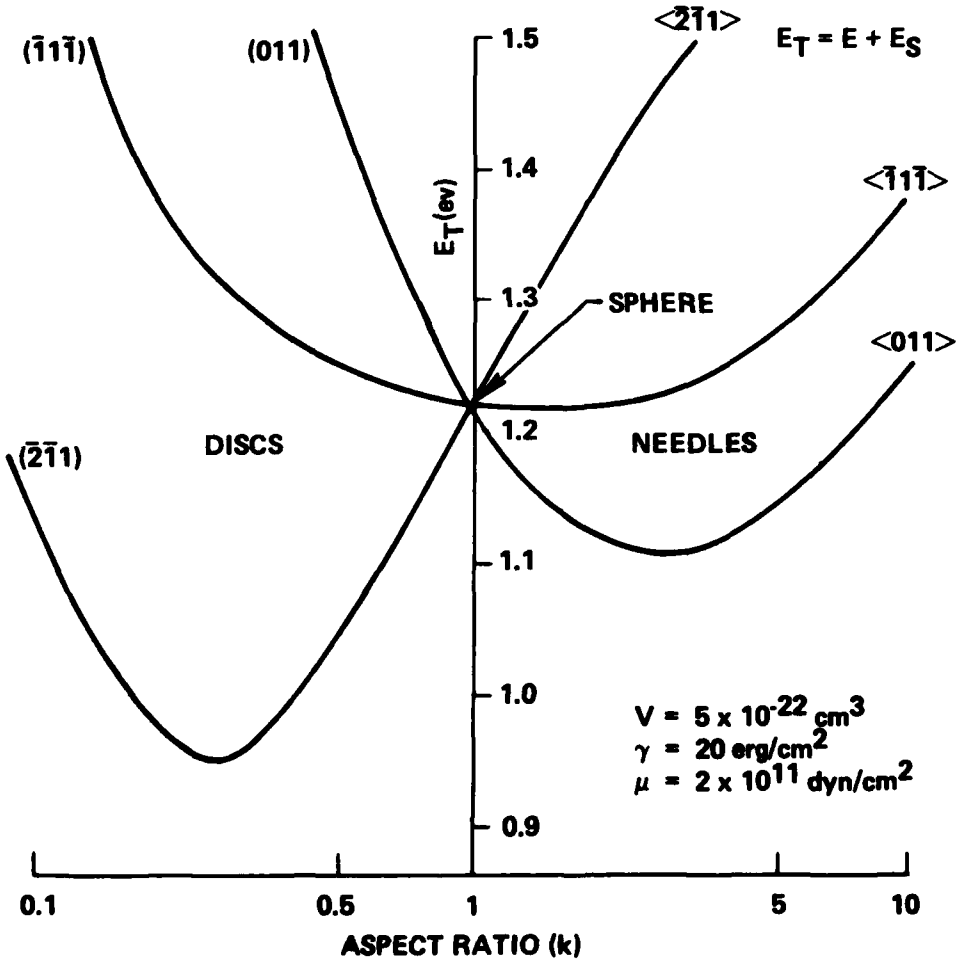

Fig. 9 The sum of E and the interfacial energy, E_T, against k.

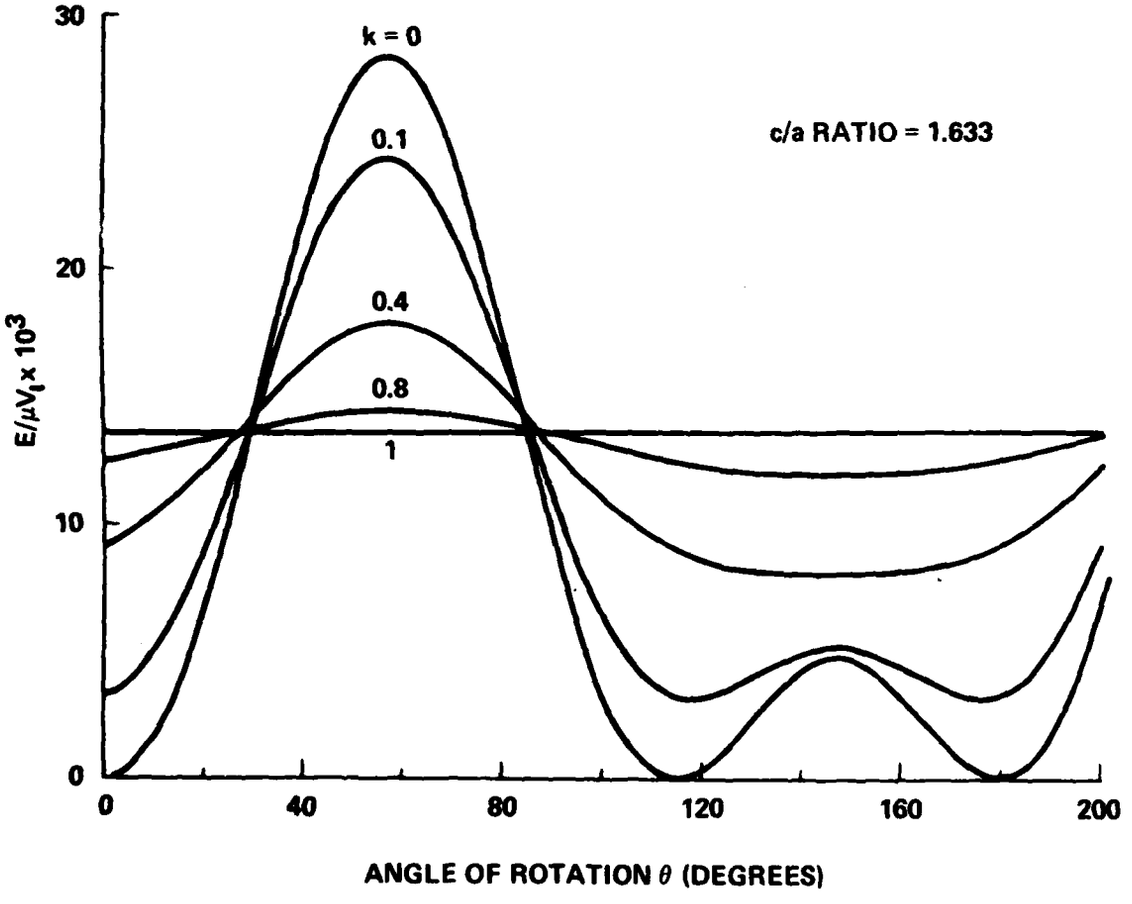

Fig. 10 The variation of E due to rotation about the x_3 axis, using e^t_{ij} of Eq. (10). k values are given in the figure, and $\theta = 0$ corresponds to $[\bar{2}\bar{1}1]$-disc and $\theta = 90°$ to $[1\bar{1}1]$-disc.

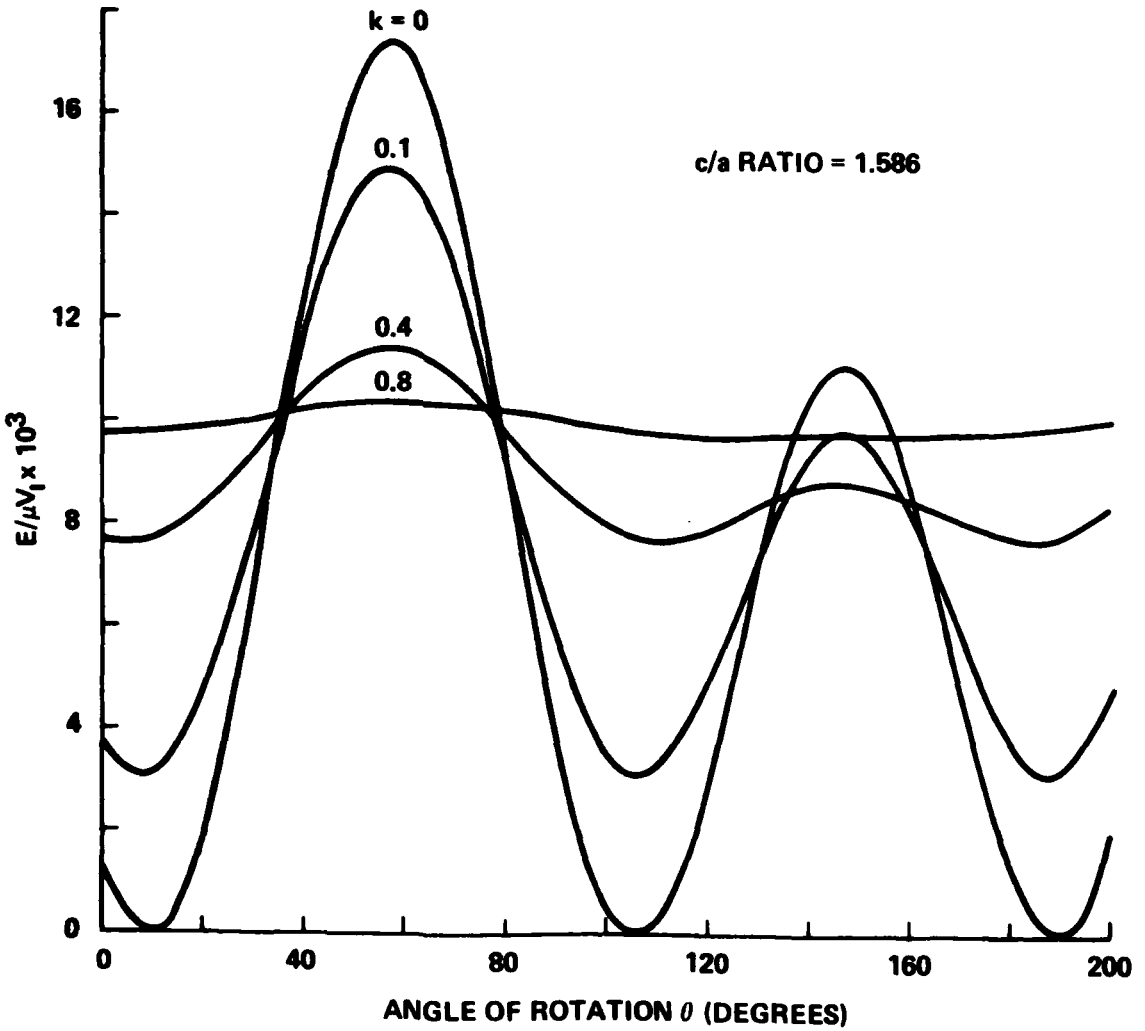

Fig. 11 The variation of E due to rotation about the x_3 axis, using e_{ij}^t of Eq. (11).

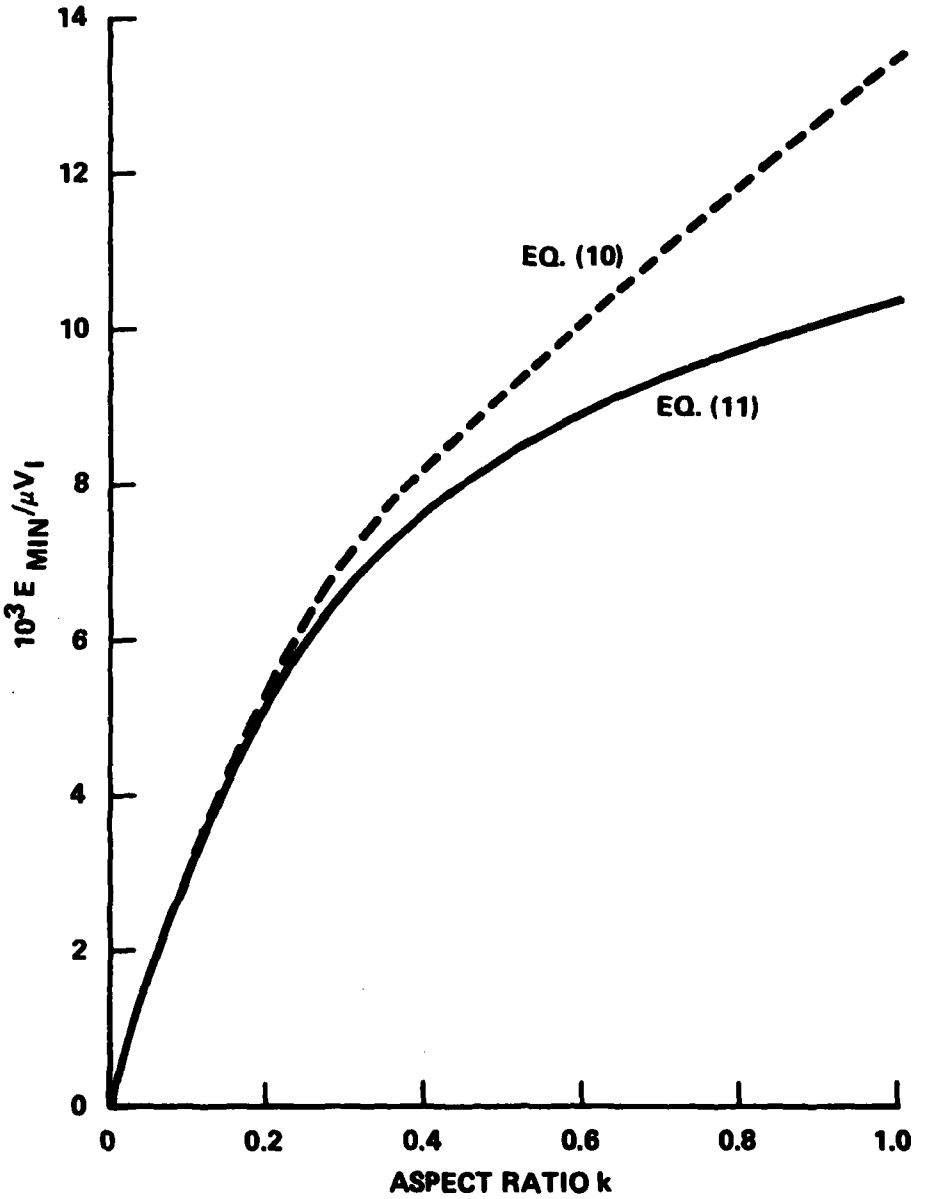

Fig. 12 The k-dependence of E_{min}. e^t_{ij} used is indicated.

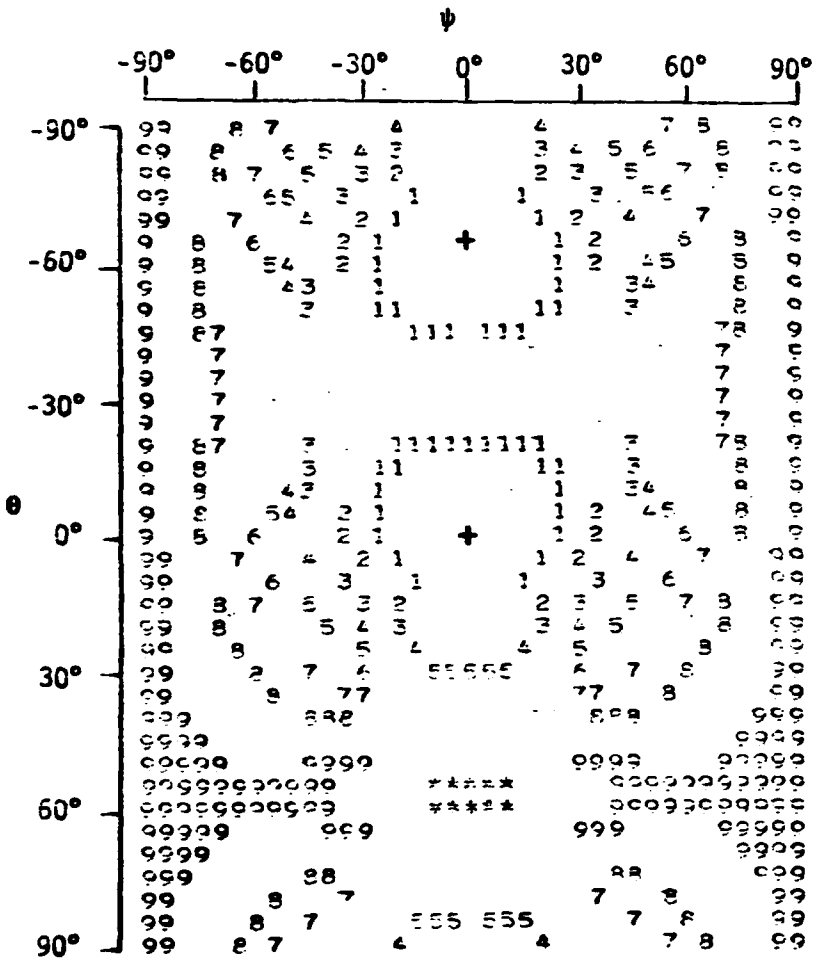

(a) k = 0

(*) $E_{max}/\mu V_I = 2.8 \times 10^{-2}$

(+) $E_{min}/\mu V_I = 0$

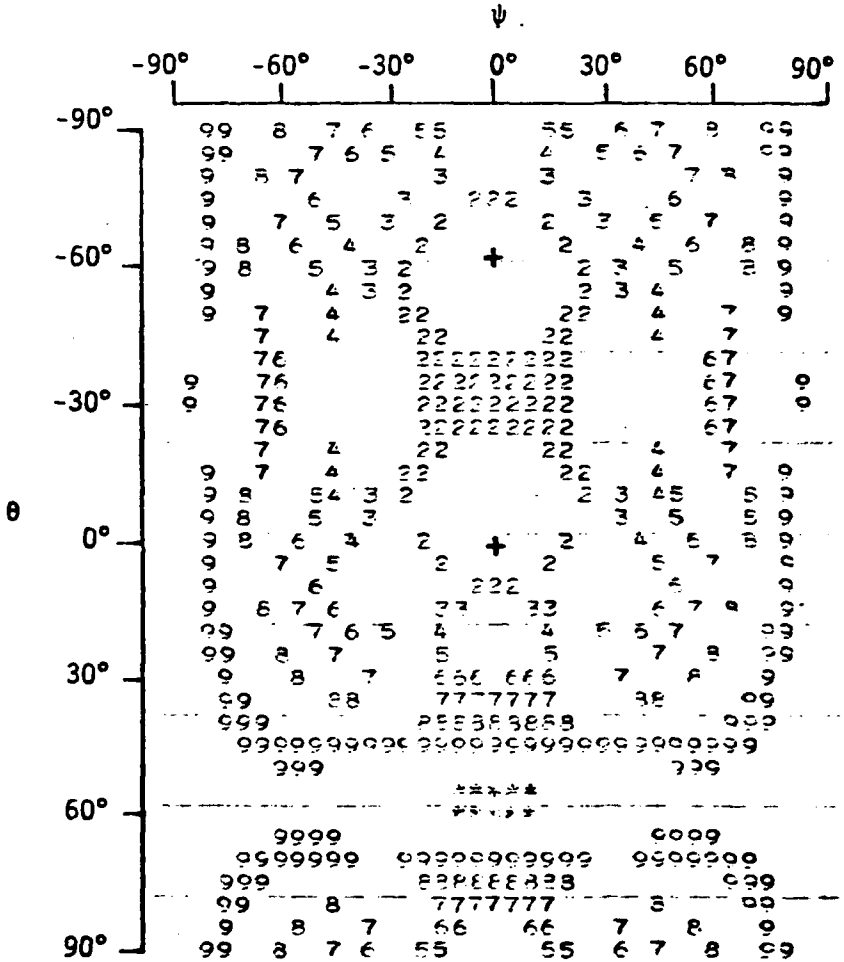

(b) k = 0.1

(*) $E_{max}/\mu V_I = 2.42 \times 10^{-2}$

(+) $E_{min}/\mu V_I = 3.16 \times 10^{-3}$

Fig. 13 The strain energy mapping with respect to θ and ψ. e^t_{ij} is given by Eq. (10). E_{max} locations are given by (*) and E_{min} by (+). (a) k = 0 (b) k = 0.1.

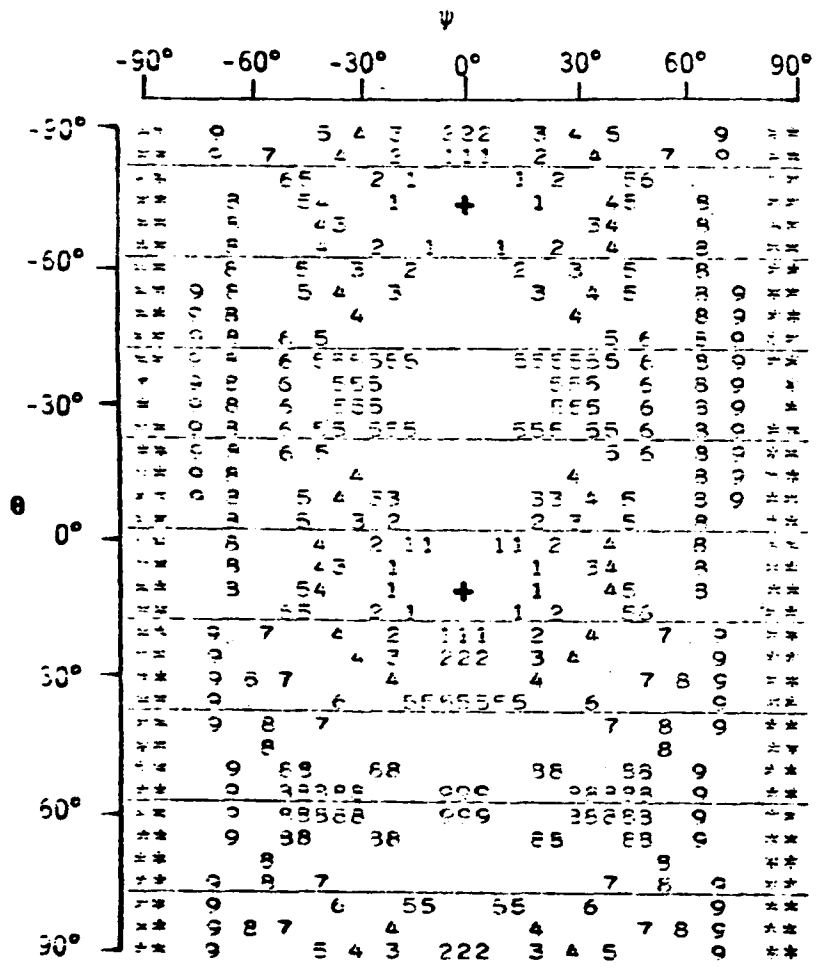

(a) k = 0

(*) $E_{max}/\mu V_I = 1.92 \times 10^{-2}$

(+) $E_{min}/\mu V_I = 0$

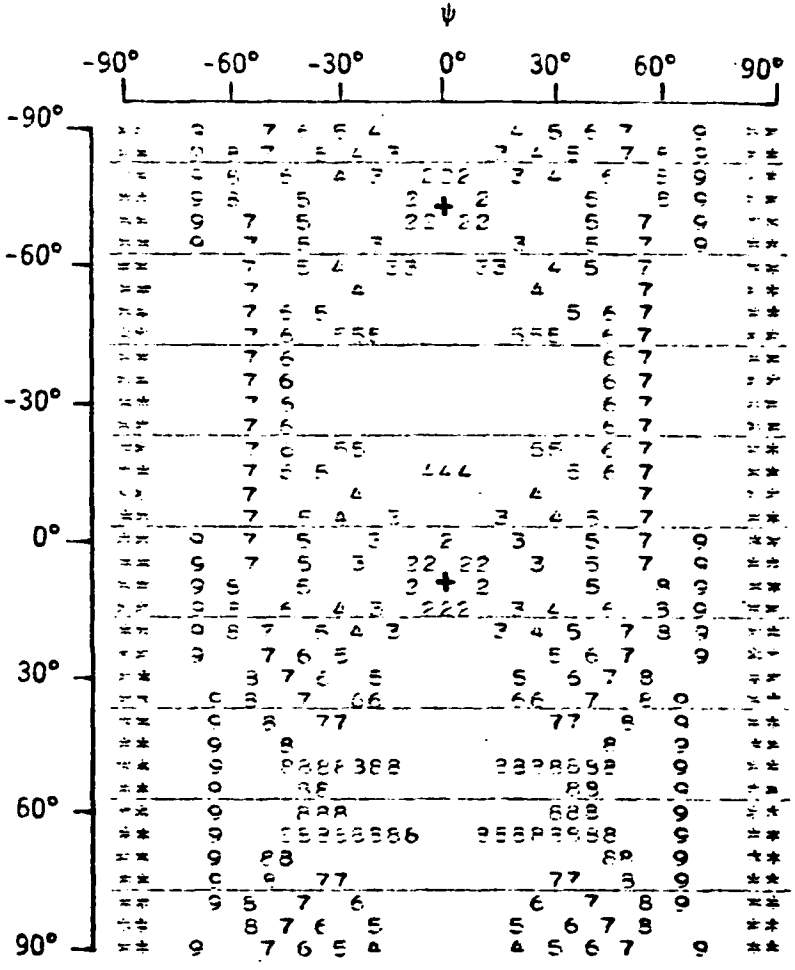

(b) k = 0.1

(*) $E_{max}/\mu V_I = 1.71 \times 10^{-2}$

(+) $E_{min}/\mu V_I = 3.05 \times 10^{-3}$

Fig. 14 The strain energy mapping using e_{ij}^t of Eq. (11). (a) k = 0, (b) k = 0.1 (c) k = 0.4 (d) k = 0.8.

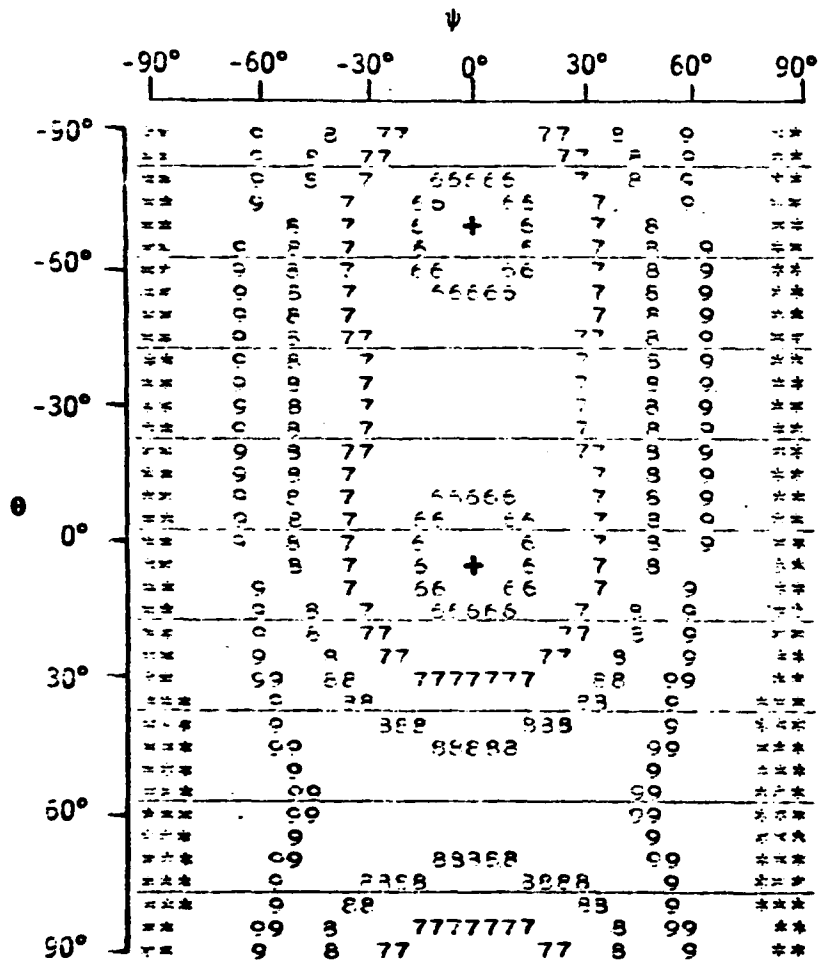

(c) k = 0.4

(*) $E_{max}/V_I = 1.33 \times 10^{-2}$

(+) $E_{min}/V_I = 7.62 \times 10^{-3}$

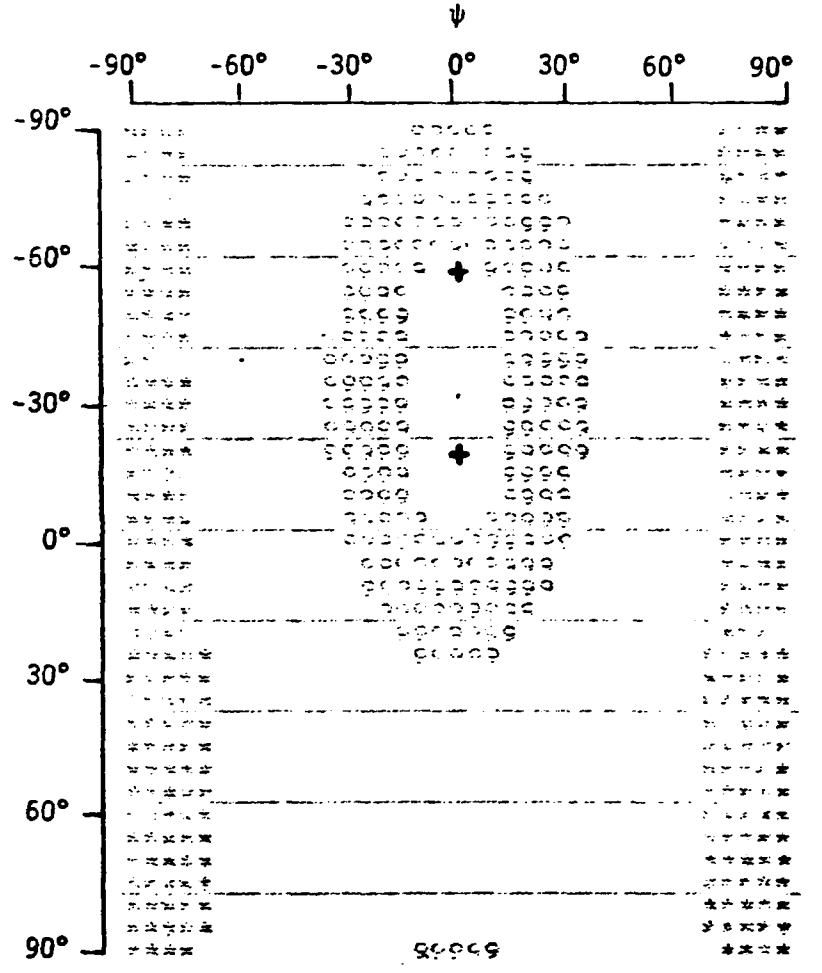

(d) k = 0.8

(*) $E_{max}/V_I = 1.09 \times 10^{-2}$

(+) $E_{min}/V_I = 9.68 \times 10^{-3}$

Fig. 14 (Cont'd)

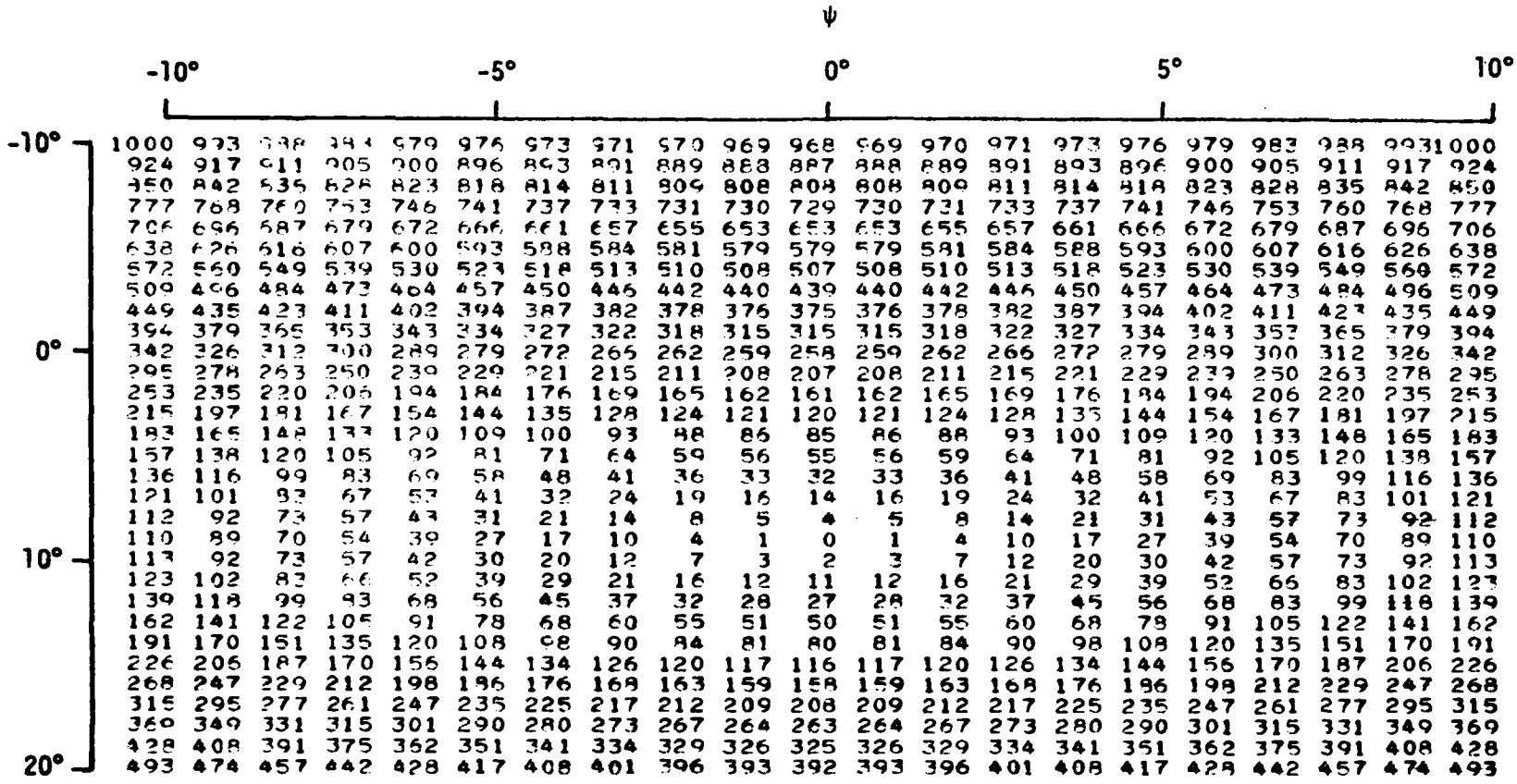

$k = 0 \qquad e^{t}_{ij}$--Eq. (11)

Fig. 15 Details of Figs. 14a and b, in the vicinity of $\theta = \psi = 0$.

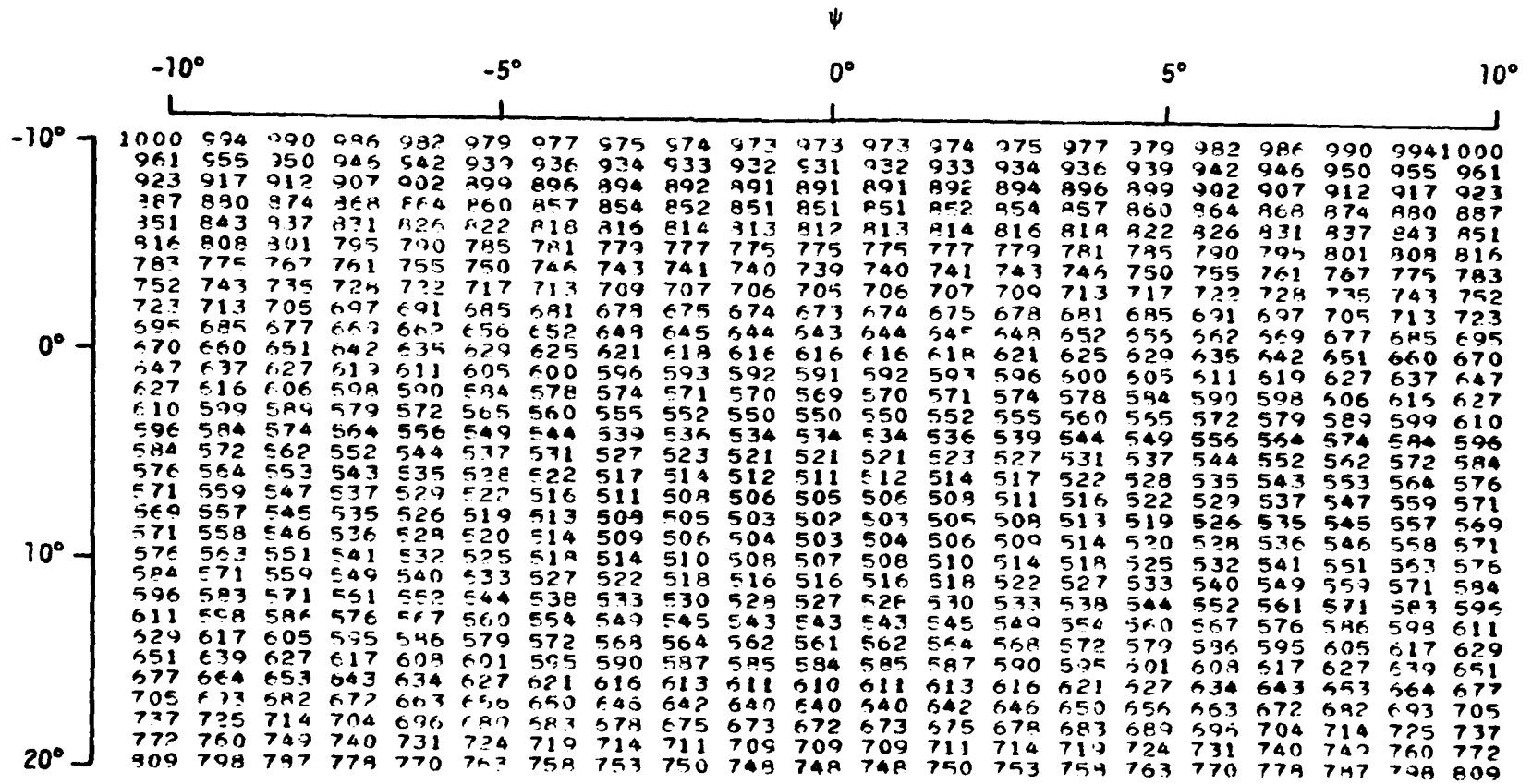

$k = 0.1 \quad e_{ij}^{t}$--Eq. (11)

Fig. 15 (Cont'd)

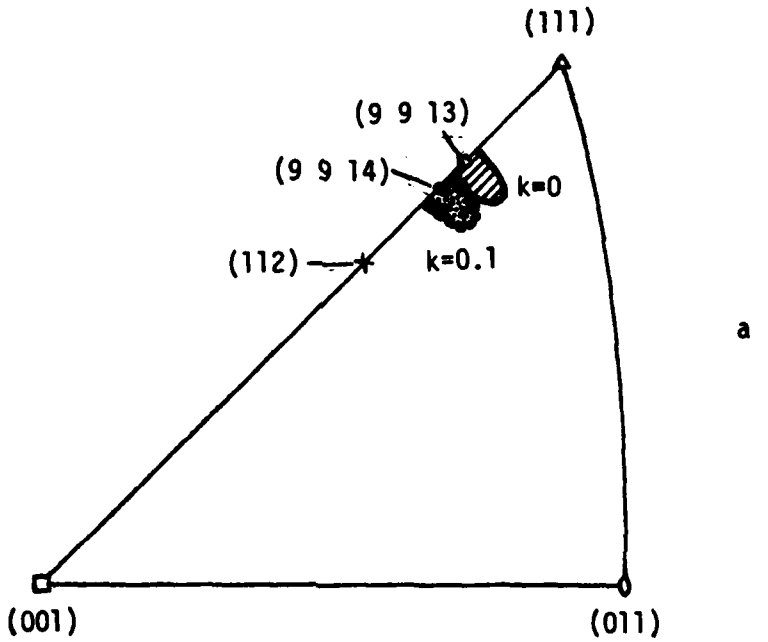

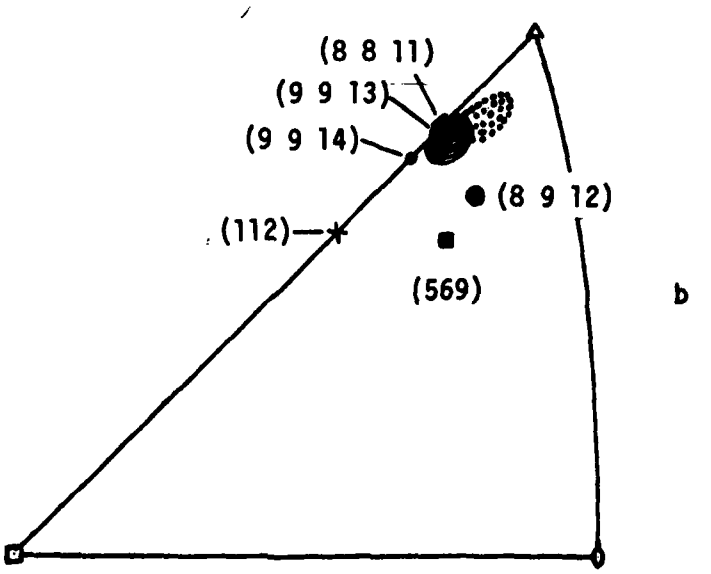

Fig. 16 (a) Habit planes predicted by the present theory
(b) Experimentally determined habit planes.


DATE
ILME